Mineralium Deposita (2024) 59:85–108
https://doi.org/10.1007/s00126-023-01183-x

ARTICLE

The geology, geochemistry, and magmatic evolution of the Legris Lake mafic–ultramafic complex, Ontario, Canada

Wyatt M. Bain[1,2] · Pete Hollings[1] · Lionnel M. Djon[3] · Matthew J. Brzozowski[1,2] · Daniel Layton-Matthews[4] · Agatha Dobosz[4]

Received: 18 October 2022 / Accepted: 23 May 2023 / Published online: 9 August 2023

Abstract

The Archean Legris Lake mafic–ultramafic complex (LLC) is spatially (~ 12 km east) and temporally (2690.59 ± 0.77 Ma) associated with the world-class Lac des Iles (LDI) palladium deposit. Modeling of whole-rock major-element compositions suggests that this complex, previously interpreted as gabbroic, is gabbronoritic in composition, adding to the likely association between LDI and the LLC. Mantle normalized trace-element profiles and modeled parental melt compositions from the cumulate lithologies indicate initial melt extraction from a metasomatized mantle source in an arc setting and subsequent crystallization of olivine, orthopyroxene, and plagioclase at depth following assimilation of SiO_2 and S from tonalitic country rock. External S assimilation contributed to sulfide saturation at depth prior to or during emplacement, but sulfide melt entrainment in intruding magmas and its retention at the site of emplacement was variable. These interpretations are supported by (1) variations in Cu/Pd ratios between PGE-rich and PGE-poor lithologies, (2) the strongly negative Eu/Eu* of paragenetically early lithologies, (3) the overlap between whole-rock $\varepsilon Nd_{(T)}$ values of LLC lithologies and Wabigoon tonalite, and (4) the positive $\delta^{34}S$ and uniformly non-zero $\Delta^{33}S$ values of magmatic sulfides. During emplacement the intruding melts also assimilated metasedimentary country rock. This effect likely became more pervasive during later stages and resulted in additional melt fractionation and inheritance of the trace-element signature of the metasedimentary country rock by the intruding magmas. This assimilation does not, however, seem to have been an important driver of sulfide saturation in this system.

Keywords Ore deposit—Layered mafic intrusions—Ni-Cu-PGE · Archean · Sm-Nd isotopes—Multiple sulfur isotopes

Introduction

A key part of meeting future demand for platinum-group elements (PGE) is exploration and development of layered mafic intrusions, and the development of petrologic models that can contextualize the source (Maier et al. 2003; Barnes and Picard 1993), tectonic setting (Naldrett 2004, 2011; Barnes et al. 2016), and magmatic evolution of these systems (Fiorentini et al. 2010; Naldrett 2011; Mungall 2014). The Legris Lake mafic–ultramafic complex (LLC) is one such layered intrusive system located in northwestern Ontario, Canada, ~ 81 km north-northwest of Thunder Bay and ~ 12 km southeast of the world-class Lac des Iles (LDI) PGE deposit (Fig. 1). This system comprises the easternmost extent of an ~ 30-km-wide, ring-shaped array of variably hornblende-rich, mafic–ultramafic intrusions located in the Archean Superior Province. These include the Tib Lake, Demars Lake, Wakinoo Lake, Tomle Lake, Buck Lake, Taman Lake, and Dog River intrusions (Sutcliffe 1986; Stone et al. 2003; hereafter referred to as the Lac des Iles Intrusive Suite). These intrusive systems are spatially related to the LDI system (Djon et al. 2018; Gupta and Sutcliffe 1990), and show textural, petrologic, and geochemical similarities that suggest a cogenetic relationship (Stone et al. 2003) and similar potential for hosting LDI-style PGE mineralization.

Editorial handling: W. D. Maier

✉ Wyatt M. Bain
wyatt.bain@gov.bc.ca

[1] Department of Geology, Lakehead University, 955 Oliver Rd, Thunder Bay, Ontario P7B 5E1, Canada

[2] British Columbian Geological Survey, 1810 Blanshard St, Victoria, BC V8T 4J1, Canada

[3] Impala Canada, 69 Yonge Street, Suite 700, Toronto, Ontario M5E 1K3, Canada

[4] Department of Geological Sciences and Geological Engineering, Queen's University, Kingston, Ontario K7L 3N6, Canada

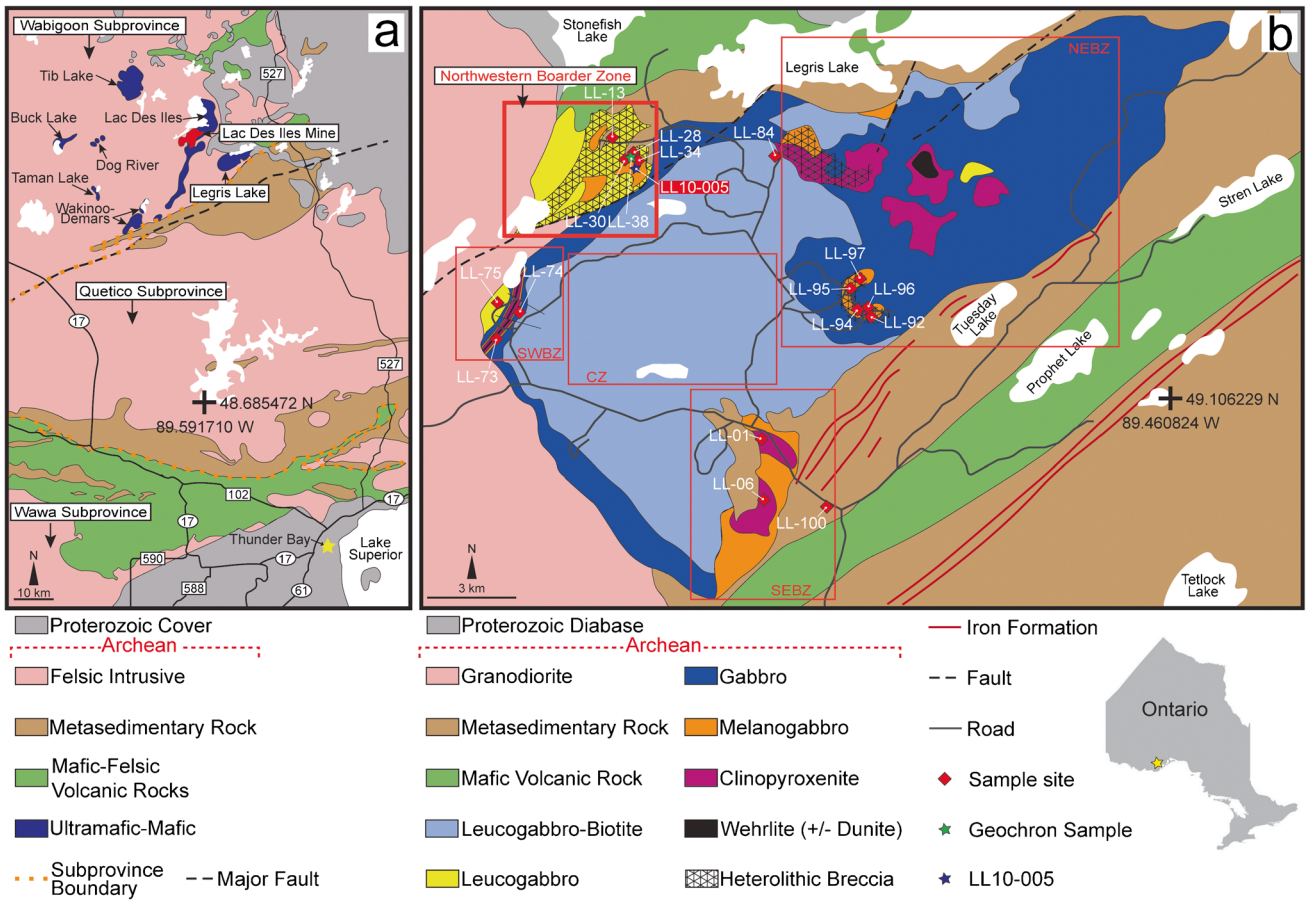

Fig. 1 **a** Regional geologic map showing locations of Thunder Bay, the Lac des Iles (LDI) mine (in red), and the Lac des Iles intrusive suite (in blue). **b** Geologic map of Legris Lake Intrusive Complex (after Pettigrew and Hattori 2002). Geologic domains are outlined with gray dotted lines and include the Northeastern Border Zone (NEBZ), Southeastern Border Zone (SEBZ), Central Zone (CZ), Southwestern Border Zone (SWBZ), and Northwestern Border Zone (NWBZ). Location of study area is denoted with a yellow star on the gray inset image (lower right)

Preliminary mapping, sampling, and exploration drilling in and around the LLC between 1999 and 2010 (Pettigrew and Hattori 2001, 2002; North American Palladium Ltd.) showed that this complex is associated with deep regional structures (i.e., tectonic sutures), contains large breccia-hosted zones of sulfide mineralization, and contains 0.5–1m-thick zones at depth with Pd grades as high as 4.5 ppm and Pd/Pt up to 23.6 (median of 2; Impala Canada Ltd.; Pettigrew and Hattori 2002). These features are consistent with the criteria recommended by Djon et al. (2018) for PGE exploration in and around the LDI system and, together, are indicative of a high degree of PGE prospectivity for the LLC relative to the other intrusions in the LDI intrusive suite.

Pettigrew and Hattori (2001, 2002) present a model for the LLC involving crystallization of olivine and orthopyroxene at depth, and subsequent emplacement of an evolved silicate magma that underwent sulfide saturation via external S assimilation from metasedimentary country rock. Here we further evaluate this model using new petrographic, geochemical, isotopic (Sm–Nd and multiple sulfur isotopes), and geochronologic (U–Pb) data sets, and present a detailed analysis of the source, setting, and role of crustal contaminants in driving the magmatic evolution of the LLC.

Geology of the Legris Lake mafic–ultramafic complex

Previous descriptions of the geology of the LLC have been provided by Pettigrew and Hattori (2001, 2002), and are briefly described here. The LLC has a surface exposure of ~ 19.5 km^2 and is situated near the Eastern margin of the Archean Wabigoon Subprovince (Superior Province) along its tectonic suture with the Quetico Subprovince (Fig. 1a). The igneous rocks of the Wabigoon Subprovince are subdivided into tonalites (~ 3 Ga), granitoid complexes

(2732–2708 Ma), and post-tectonic granitoid stocks (2709–2685 Ma; Blackburn et al. 1991). The latter group includes several ~ 2.69-Ga mafic–ultramafic complexes that intrude earlier granitic–tonalitic lithologies of the Wabigoon Subprovince (Blackburn et al. 1991; Sutcliffe et al. 1989). The mafic–ultramafic intrusive complexes of the LDI Intrusive Suite are likely part of this group (Pettigrew and Hattori 2001).

Along its northern, southern, and eastern margins, the LLC is bordered by greenschist-facies metasedimentary and metavolcanic rocks of the Quetico Subprovince (Fig. 1b). The Quetico metavolcanic rocks are basaltic in composition and only contact the LLC along its northern boundary. The metasedimentary rocks are primarily greywackes, siltstones, conglomerates, and minor oxide-facies iron formations (Pettigrew and Hattori 2002) that are commonly interbedded with or crosscut by mafic metavolcanic rocks. Together these lithologies comprise part of an accretionary complex (Percival and Williams 1989) that formed during collision of the Wawa–Abitibi and Wabigoon terranes at ~ 2.696 Ga following docking of the Wabigoon and Winnipeg River terranes at ~ 2.7 Ga. The country rocks around the LLC contain well-developed NE-trending space cleavage that is associated with this accretionary episode (Williams 1990) and is overprinted by N-trending Midcontinent Rift-related fracture sets (~ 1100 Ma; Paces and Miller 1993). The intrusive rocks of the LLC are crosscut by the N-trending fracture sets but lack NE-trending space cleavage. This relationship roughly brackets the formation of the LLC between the accretion of the Wabigoon and Quetico Subprovinces and formation of the Midcontinent Rift (Pettigrew and Hattori 2001, 2002).

The LLC is composed primarily of gabbroic cumulate lithologies and scattered ultramafic occurrences (Fig. 1b). Most of the central and western portions of the LLC are covered by a biotite-rich variety of leucogabbro (plagioclase > pyroxene) that cross cuts a central mass of more mafic gabbro (plagioclase = pyroxene). Along the northern and western boundaries of the complex, biotite-poor leucogabbro and gabbro dominate, and are the main host for sulfide mineralization. In the eastern and southern half of the complex, gabbro surrounds isolated pods of melanogabbro (plagioclase < pyroxene) and clinopyroxenite, which contain small zones of ultramafic dunite and wehrlite that comprise the only olivine-bearing rocks in the complex (encountered during exploration drilling; Pettigrew and Hattori 2001, 2002). To the south, biotite-bearing leucogabbro is in sharp contact with an isolated mass of melanogabbro–clinopyroxenite and a large roof pendant of Quetico metasedimentary rock (Fig. 1b). Based on the distribution of these lithologies, Pettigrew and Hattori (2001, 2002) divided the LLC into five domains — the Central Zone (CZ), Southwestern Border Zone (SWBZ), Southeastern Border Zone (SEBZ), Northeastern Border Zone (NEBZ), and Northwestern Border Zone (NWBZ; Fig. 1b). These geologic domains are described in detail in Supplementary Material ESM1.

Sulfide-associated PGE mineralization in the LLC is concentrated in the fault-bounded Northwestern Border Zone (Fig. 1b). This area is primarily composed of biotite-poor leucogabbro and country rock-bearing heterolithic breccia, but exhibits significant variability in the texture, composition, degree of alteration, and sulfide content over areas of < 5 m. For example, a 70-m transect through this area might encounter partially melted metaconglomerate (Fig. 2a), partially assimilated xenoliths of amphibolite-grade metasedimentary rock (Fig. 2b, c), altered leucogabbro with primary magmatic layering (Fig. 2d), deformed clinopyroxenite breccia fragments in a leucogabbro matrix with well-developed flow textures (Fig. 2e), pods of sulfide mineralization (Fig. 2f), and cross-cutting zones of variably mineralized intrusive rocks showing textures indicative of high-temperature deformation (Fig. 2g, h). This complexity is also present at depth, with structures, textures, and rock types observed in drill core displaying little continuity with those observed at the surface (Pettigrew and Hattori 2002; North American Palladium Ltd.). The large compositional and textural diversity of this area is indicative of a dynamic igneous environment involving repeated episodes of silicate melt injection, host rock brecciation and deformation, and extensive interaction with country rocks (Pettigrew and Hattori 2002). This latter point is illustrated by the presence of abundant metasedimentary xenoliths in the LLC that exhibit textural features indicative of partial melting and assimilation (Pettigrew and Hattori 2002) such that xenoliths commonly grade into the intrusive rocks (Fig. 2a, b).

The central portion of the Northwestern Border Zone contains the greatest abundance of PGE-bearing sulfide mineralization in the LLC (Pettigrew and Hattori 2002; Impala Canada Ltd.), with previous exploration drilling intersecting multiple mineralized intervals (1 m or more) containing > 1 ppm Pd (up to 4.5 ppm Pd in hole LL01-14, median Pd/Pt of 1.2; Pettigrew and Hattori 2002). Additional drilling focused on the southern portion of the Northwestern Border Zone by North American Palladium Ltd. produced several holes with up to 2.25 ppm Pd (average 0.1) and average Pd/Pt of 2.73 (up to 27). This is less than the mineralized zones in the Mine Block Intrusion at LDI (average Pd concentration of 0.5–3.0 ppm and average Pd/Pt of 7–14; North American Palladium Ltd.), but comparable to ultramafic rocks in the northern extent of the LDI system (Djon et al. 2018).

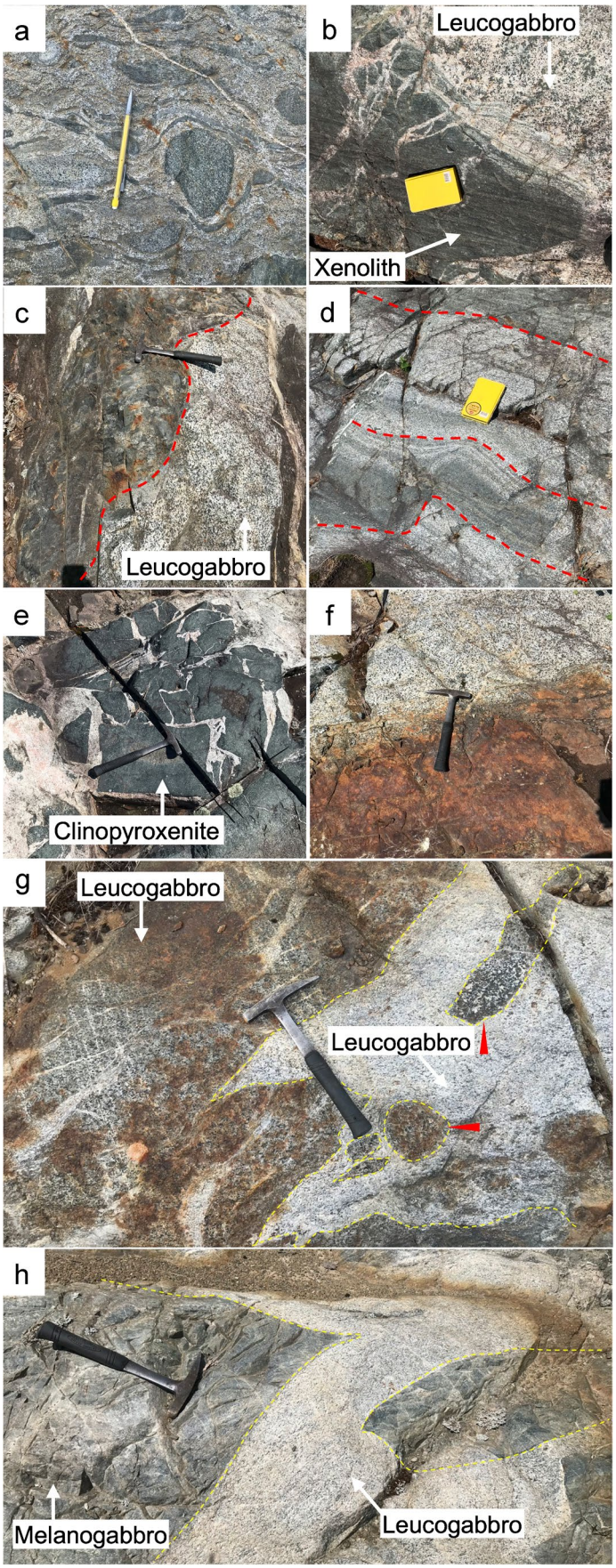

Fig. 2 Outcrop photos of the Northwestern Border Zone of the Legris Lake Complex. **a** Partially melted metaconglomerate, with matrix material completely consumed by silicate melt. **b** Partially assimilated Quetico metasedimentary xenolith in leucogabbro. Note the reaction rim around the xenolith. **c** Contact between metasedimentary rock (left) and leucogabbro (right). Contact denoted by a red dotted line. **d** Leucogabbro with primary magmatic layers of pyroxene-rich melanogabbro (outlined in red). **e** Clinopyroxenite breccia with leucogabbro matrix. **f** Oxidized, sulfide-bearing zone in leucogabbro. **g** Mineralized leucogabbro crosscut by later, unmineralized leucogabbro (denoted by yellow dotted line). Note the fragments of mineralized leucogabbro (red arrows) in the cross-cutting leucogabbro. **h** Partially deformed melanogabbro crosscut by later leucogabbro. Note the tapered ends of the melanogabbro masses that indicate partial solidification and subsequent deformation by the intruding leucogabbro

Methods

Sampling and preparation

A total of 100 samples were collected from surface localities throughout the LLC that were mapped and excavated as part of previous exploration and drilling campaigns in the early 2000s. A representative sample set of the major lithologies present in the LLC was collected from outcrops in each of the five major geologic domains of the LLC. It should be noted, however, that some rock types that were identified during previous exploration activities, but which represent volumetrically minor components of the intrusive suite within the LLC system (e.g., anorthosite, dunite, gabbrodiorite, and websterite), were not observed in outcrop and, thus, not sampled as part of this study. In addition, 60 samples of drill core that crosscut an ~ 527-m-long segment of sulfide- and PGE-bearing mafic cumulates (i.e., drill hole LL10-005, 47–527 m; Fig. 1) in the Northwestern Border Zone were also collected as part of this study. Relative to the highly variable suite of lithologies present in the Northwestern Border Zone, drill hole LL10-005 contains intervals of up to 60 m in which the rock types are continuous, well preserved, and ideal for petrographic and isotopic characterization. Following sample collection, a representative set of polished thin sections was prepared using the in-house rock preparation facility at Lakehead University.

Analytical methods

Analytical methods include petrography, whole-rock geochemistry, U–Pb geochronology, whole-rock Sm–Nd isotope analysis, in situ multiple S isotope analysis of sulfides via secondary ion mass spectrometry, and scanning electron microscope–mineral liberation analysis (SEM-MLA). Detailed descriptions of these methods are presented in the Supplementary Material ESM1.

Results

Petrography of the major rock types in the LLC system

The LLC contains a wide variety of rock types ranging from mafic–ultramafic cumulate rocks to amphibolite-facies volcanic and siliciclastic metasedimentary rocks. Table 1 summarizes the modal mineralogy of each lithology and accompanies a more detailed description of each lithology in ESM1 and previous work by Pettigrew and Hattori (2001, 2002).

The cumulate lithologies of the LLC are primarily plagioclase- and clinopyroxene-rich orthocumulate to adcumulate gabbros (Fig. 3a–c; ESM1, Fig. 1a–g), clinopyroxenite (Fig. 3d; ESM1, Fig. 1f, h), and minor volumes of other ultramafic lithologies (not observed). Here we differentiate the gabbroic rocks of the LLC based on the relative abundance of plagioclase and pyroxene into leucogabbro (Fig. 3a, b), gabbro, and melanogabbro (Fig. 3c) subvariants. The eastern half of the complex is primarily mesocumulate gabbro (Fig. 1b) that surrounds isolated masses of melanogabbro and clinopyroxenite. The western half of the complex is dominantly unaltered, adcumulate to mesocumulate leucogabbro, with abundant primary biotite and minor intergranular orthopyroxene (hereafter referred to as biotite-leucogabbro; Fig. 3b). This biotite-leucogabbro variant cross-cuts all other igneous lithologies and is paragenetically the youngest intrusive unit.

Platinum-group element-rich sulfide mineralization in the LLC is localized to the Northwestern Border Zone and is primarily hosted in a biotite-poor leucogabbro (Table 1), referred to hereafter as leucogabbro. This unit occurs in outcrop as finely layered masses with 1–10-cm-wide bands of melanogabrro and clinopyroxenite (Fig. 2b) and as matrix in heterolithic breccias. Sulfide mineralization occurs primarily as net-textured (Fig. 3e, f) and disseminated pyrite and chalcopyrite, with minor pyrrhotite and pentlandite (ESM1, Fig. 2a–f) and commonly comprises up to 5 vol% or more of the modal mineral abundance. Mineralized zones are typically surrounded by green alteration halos and orange sulfide weathering in outcrop (Fig. 2f, g), and are invariably associated with ilmenite, magnetite (Fig. 3f), and intercumulus biotite and quartz in thin section (ESM1, Fig. 2a). Though not observed in this study, platinum-group minerals (PGM; Pd-Bi and Pt–Pd-Bi tellurides) are associated with Cu–Ni sulfides (Pettigrew and Hattori 2002). Outside of the Northwestern Border Zone, PGE-bearing sulfide mineralization is mostly absent or limited to small, isolated showings.

Much of the LLC is overprinted by hydrous alteration that is expressed as uralitization of primary pyroxene to hornblende–actinolite–chlorite–epidote–talc and sericitization of primary plagioclase. This alteration is most pervasive in the Northwestern Border Zone where primary pyroxene and plagioclase are commonly only discernable as hornblende and sericite pseudomorphs (ESM1, Fig. 1h). In contrast, the paragenetically late biotite-leucogabbro is relatively unaltered (Fig. 2b; ESM1, Fig. 1c–e).

Table 1 Summary of major lithologies in the LLC describing modal mineralogy of cumulate and intercumulate mineral phases

Lithology	Description of observed composition*,†	Comments
Leucogabbro (LGAB)	Cumulus plagioclase (~60–75%) and cpx (~15–40%) with intergranular quartz (~1–5%) and biotite (~1–5%; up to ~10% locally). Up to ~5% sulfides, when observed. Includes course-grained varitextured varieties	Main host for sulfide mineralization
Biotite-leucogabbro (LGAB-Bio)	Cumulus plagioclase (~60–65%), ophitic cpx (~15–18%), euhedral opx (~10–12%), apatite- and zircon-bearing biotite (~5–15%), and quartz (~<5%)	Least altered and paragenetically latest intrusive phase
Gabbro (GAB)	Cumulus plagioclase (~40–50%) and cpx (~40–50%) with variable intergranular quartz and apatite- and zircon-bearing biotite (up to ~15% total). Sulfide/oxides are commonly < 1% but can be up to 5% in the Northwestern Boarder Zone	Comprises most of the LLC
Melanogabbro (MGAB)	Cumulus cpx (~50–70%) and plagioclase (30–40%) with minor intergranular quartz and magnetite (~<15%, total). Sulfide mineralization is < 2% when observed	Occurs as segregated bands in layered lithologies or as isolated masses
Clinopyroxenite (CPXTY)	Cumulus cpx (~90–95%) and plagioclase (<5%) with intergranular biotite (<5%). Sulfide mineralization is < 1% when observed	Occurs as segregated bands in layered lithologies or as isolated masses
Quetico metasedimentary rocks (MTSD)	Arkose sandstone, siltstone, graywacke, coarse pebble conglomerate, banded volcaniclastic rock, and iron formations. Commonly occurs as a component of heterolithic breccias or as xenoliths and roof pendants	Altered to amphibolite facies along the LLC's periphery
Alteration	Hydrous alteration involving the uralitization of primary cpx/opx and sericitization of primary plagioclase. Pyroxene pseudomorph of hornblende–actinolite–chlorite–epidote–talc and sericite pseudomorph of plagioclase are common in heavily altered lithologies	Pyroxene throughout the complex are significantly more altered than plagioclase

*Estimated modal abundances observed in transmitted light represent the observed abundance of primary phases plus alteration products (i.e., amphibole, sericite, talc, chlorite, epidote) that occur either within partly altered primary mineral phases or as pseudomorphs. It should be noted that orthopyroxene (opx) was only directly observed in biotite-leucogabbor, but is likely to comprise up to 40% of the total pyroxene abundance that occur along with clinopyroxene (cpx). See discussion for details

†All modal abundances reported in vol%

Petrography and chemostratigraphy of layered intrusive rocks in the LLC

Drill hole LL10-005 samples a continuous interval of sulfide-bearing cumulate rock. The dominant rock type here is orthocumulate leucogabbro, with well-preserved, horizontally (Fig. 2d) oriented magmatic layering. The layering occurs in discrete packages (units) that include zones of heterolithic breccia with abundant fragments of Quetico metasedimentary rock (visible in hand sample and outcrop). Boundaries between individual units are visible in thin section and are characterized by an abrupt change in phenocryst grain size and the modal abundance of primary plagioclase and clinopyroxene at the tops and bottoms of each layer.

Individual layers commonly have more mafic lithologies (melanogabbro with intervals of clinopyroxenite) at their stratigraphic tops that grade downward into bands of mineralized gabbro and leucogabbro at their stratigraphic bottoms. This pattern is visible in downhole plots as systematic trends in MgO, CaO, Fe_2O_3, S, Cu, Ni, Pd, and Pt enrichment or depletion that are truncated or reversed at the stratigraphic tops and bottoms of each unit in a cyclic manner (Fig. 4). Five geochemical segments (referred to hereafter as cyclic units; CU) are identified in Fig. 4 between 0- and 500-m depth in drill hole LL10-005: CU1 (0–67 m), CU2 (68–136 m), CU3 (137–277 m), CU4 (278–397 m), and CU5 (398–497 m). Within a single cyclic unit, MgO, CaO, and Fe_2O_3 concentrations decrease systematically from top to bottom and track a modal increase in plagioclase abundance.

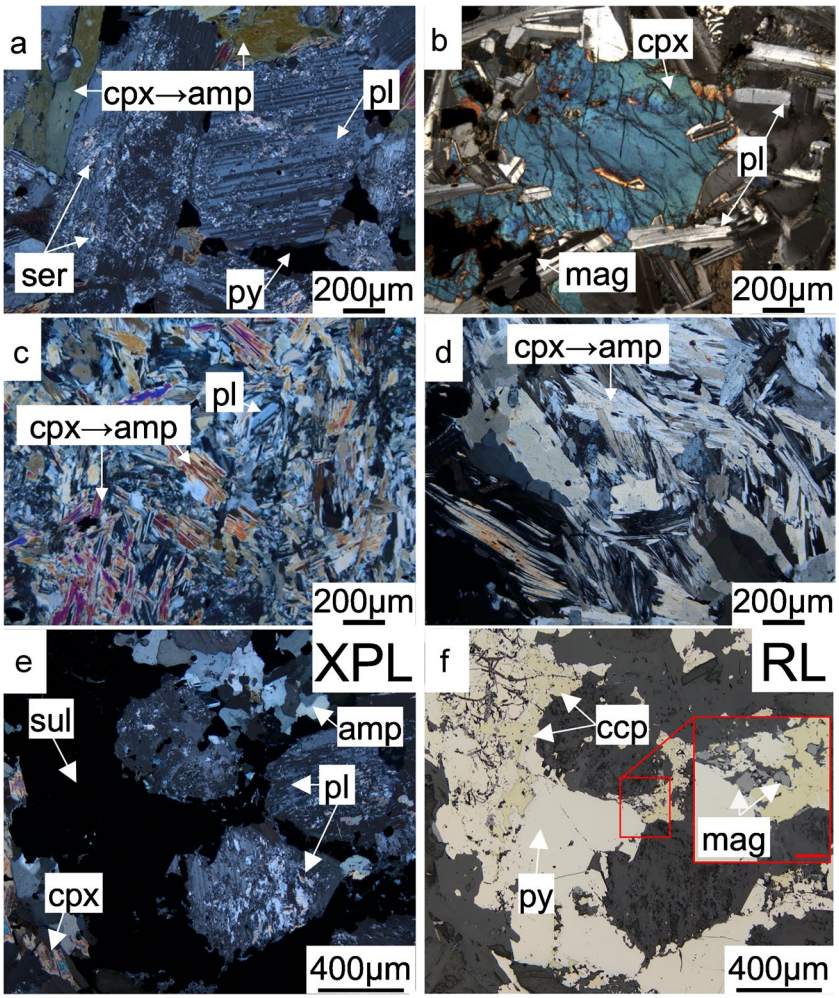

Fig. 3 Photomicrographs of cumulate lithologies from the LLC in cross-polarized light. **a** Leucogabbro showing plagioclase (pl) phenocrysts with minor sericite (ser) alteration and intergranular clinopyroxene (cpx; replaced by amphibole: amp) and pyrite (Py). **b** Biotite-leucogabbro with tightly interlocking plagioclase and ophitic clinopyroxene (cpx). Note the opaque magnetite (mag) surrounding plagioclase in the lower left-hand corner. **c** Melanogabbro with tightly interlocking plagioclase, with clinopyroxene partially replaced by amphibole. **d** Least altered clinopyroxenite showing tightly interlocking clinopyroxene altered to amphibole. Note that these images are of adcumulate varieties of major lithologies. **e** Cross-polarized photomicrograph (XPL) of plagioclase and pyroxene phenocrysts (altered to amphibole) surrounded by opaque net-textured sulfides (sul). **f** Area shown in panel "a" in reflected light showing intergrown pyrite (py), chalcopyrite (ccp), and magnetite (mag). Scale bar in inset image is 50 µm

This pattern matches the paragenesis of mineral phases in gabbroic lithologies in hand sample where plagioclase is the paragenetically earliest cumulus phase and pyroxene either surrounds plagioclase or is an intergranular phase.

Pyrite mineralization occurs throughout LL10-005 and is reflected in the high S concentrations along the length of most cyclic units (Fig. 4). However, chalcopyrite, pentlandite, and PGE mineralization is most abundant in CU1 and CU5 and is concentrated near the stratigraphic bottoms of each unit where the highest S, Cu Ni, Pd, and Pt concentrations are observed (Fig. 4). In contrast CU2–CU4 have very low concentrations of base metal sulfides and essentially no PGE mineralization. In addition, the abundance of chalcopyrite in hand sample is negatively correlated with the occurrence of metasedimentary rock xenoliths. This is the case in CU2–CU4, which commonly contained abundant metasedimentary rock fragments and have the lowest PGE, Ni, and Cu concentrations.

Geochronology of the mineralized leucogabbro

A single sample of coarse-grained leucogabbro from the Northwestern Border Zone was selected for zircon U–Pb ID-TIMS geochronology. Analytical results and transmitted-light photomicrographs of representative zircons chosen for analysis are provided in Supplementary Table 1 in ESM2. The analyzed sample yielded an abundant population of non-magnetic, skeletal, inclusion-free zircon crystals. Most grains were subhedral and elongate in form, without any well-developed facets, suggestive of relatively late, but rapid crystallization conditions.

Four of the analyzed single grain fractions contain ~ 170–600 ppm, moderate Th/U ratios (0.47–0.64), and a narrow range in $^{207}Pb/^{206}Pb$ ages, with an age of 2690.6 ± 0.8 Ma (2 SD, $n = 4$). Geochronological results for all four zircon fractions overlap and fall within the 2σ

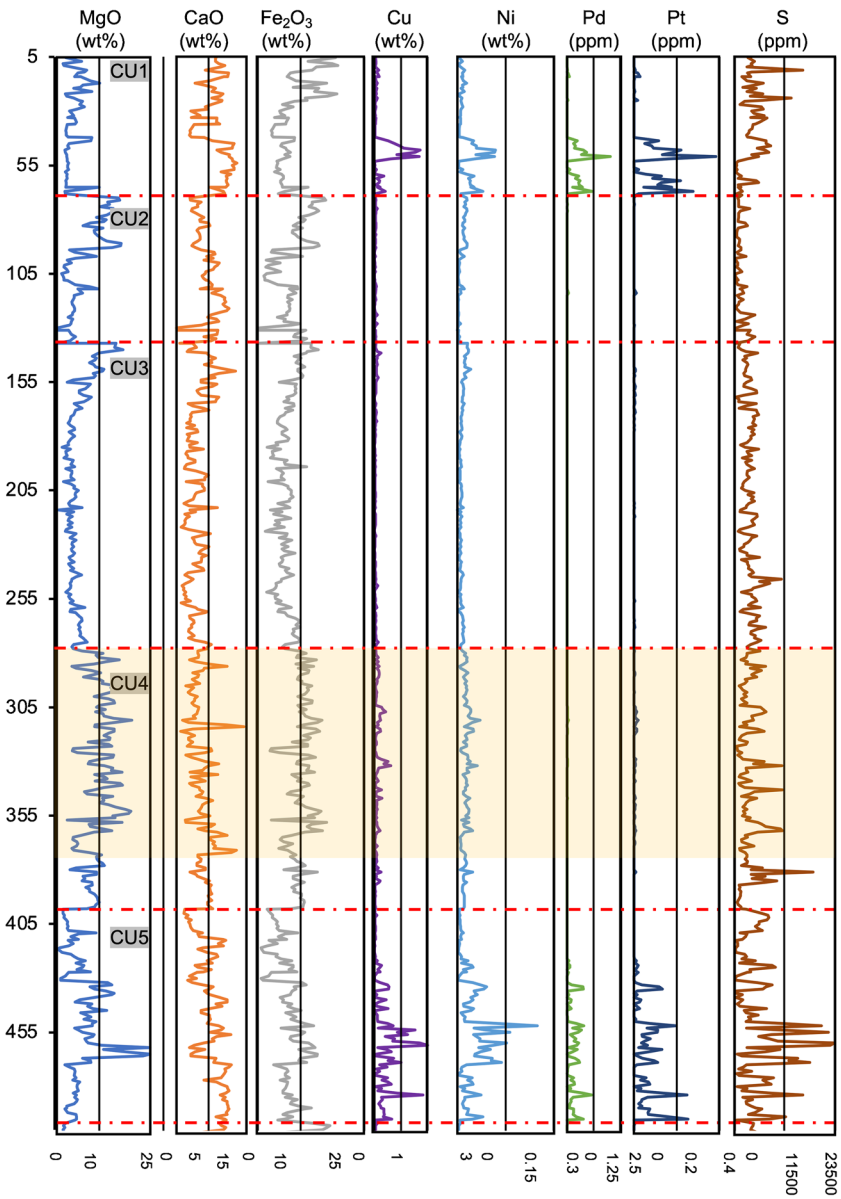

Fig. 4 Downhole plots from drill hole LL10-005. Individual layered intrusive units (cyclic units) are bracketed with red dotted lines. Note the systematic decrease in the MgO with depth in each unit (e.g., CU2 and CU3). This is related to a modal increase in plagioclase with depth. Also note the correlation between S, Ni, Cu, Pt, and Pd, indicative of base-metal sulfide and sulfide-associated PGE mineralization and a general lack of olivine in the layered units. The area highlighted in yellow contains an interval of metasedimentary rock-bearing heterolithic breccia; note the more complicated and less systematic variation in major-element compositions in this section

uncertainty limits of the Concordia band (0.0–0.2% discordant). Considering the four zircon fractions together yield a weighted average age of 2690.59 ± 0.77 Ma (MSWD = 0.1, probability of fit = 96%).

Whole-rock geochemistry

Whole-rock major and trace element geochemical data gathered form surface exposures and drill hole LL10-005 in the Northwestern Border Zone (this study and Impala Canada Ltd., geochemical data bases) are summarized in Table 2 and Supplementary Table 3 in ESM2. See Supplementary Tables 2 and 4 in ESM2 for full data set.

Generally, the major-element compositions of intrusive lithologies from the LLC fall into two distinct groups. The first group accounts for the majority of samples collected in the LLC and is visualized in CaO vs. MgO space primarily as a linear trace of data points between 5.0–15.0 wt% CaO and 4.0–16.0 wt.% MgO that intersects, and is subparallel to, the clinopyroxene–albite control line (Fig. 4a). A subset of data points systematically skews away from the trend towards a cluster of data points near the origin that closely overlaps the composition of the Quetico metasedimentary

Table 2 Summary of whole-rock geochemistry of major lithologies in the Legris Lake Complex

	CPXYT ($n=5$)			MGAB ($n=4$)			GAB ($n=121$)*			LGAB ($n=5$)			LGAB-Bio ($n=1$)	MTSD ($n=1$)	Ton ($n=1$)
	Min	Max	Med	Min	Max	Med	Min	Max	Med	Min	Max	Med			
SiO_2	40.2	55.9	46.9	49.4	51.8	50.9				48.3	64.2	50.2	56.5	68.8	66.9
Al_2O_3	4.0	15.8	9.6	13.6	15.2	14.8	1.1	20.6	3.7	12.6	20.7	19.9	14.9	13.2	15.4
Fe_2O_3	12.4	23.0	19.3	10.9	13.4	13.2	5.1	35.7	8.4	3.0	18.1	10.5	9.1	7.3	5.4
CaO	3.9	12.6	8.4	8.9	10.3	9.7	0.3	12.6	7.6	4.5	10.2	9.4	6.5	2.2	4.6
MgO	5.2	18.0	11.8	6.3	9.2	7.7	0.5	13.1	6.1	1.7	11.7	4.1	4.9	3.5	1.9
Na_2O	0.6	3.0	0.9	2.4	2.9	2.7	0.0	4.6	2.8	1.4	5.7	3.4	3.7	2.6	4.1
K2O	0.1	2.7	0.3	0.3	0.7	0.4	0.0	4.4	1.1	0.6	1.0	0.9	2.9	1.4	1.4
Cr_2O_3	0.0	0.1	0.1	0.0	0.1	0.1	0.0	0.2	0.0	0.0	0.0	0.0	0.0	0.0	0.0
TiO_2	0.8	2.8	1.3	0.8	1.1	0.8	0.0	2.5	0.7	0.3	0.7	0.6	0.8	0.7	0.5
MnO	0.1	0.3	0.2	0.2	0.3	0.2	0.0	0.2	0.1	0.0	0.2	0.1	0.1	0.1	0.1
P_2O_5	0.0	0.3	0.1	0.1	0.4	0.2	0.0	0.8	0.3	0.0	0.3	0.1	0.5	0.1	0.1
SrO	0.0	0.1	0.1	0.0	0.1	0.1	0.0	0.1	0.0	0.0	0.1	0.1	0.1	0.0	0.0
BaO	0.0	0.1	0.0	0.0	0.0	0.0	0.0	0.1	0.0	0.0	0.1	0.0	0.1	0.1	0.0
LOI	0.4	1.9	0.7	0.3	1.7	1.3				0.6	3.4	1.8	0.1	2.7	0.9
Cs	0.1	2.5	0.3	0.2	1.2	0.6				1.0	2.5	1.9	2.1	1.9	1.5
Rb	1.8	73.7	2.7	2.8	23.3	8.0				18.9	32.6	20.8	62.8	35.2	57.9
Ba	57.9	870.6	83.9	136.7	383.3	294.3	0.5	1000.0	307.0	204.1	464.6	255.1	854.4	425.2	326.0
Th	0.2	4.1	0.7	0.1	2.1	0.3				0.1	1.3	0.4	6.5	4.4	6.6
U	-	0.5	0.2	-	0.6	0.1				0.1	0.4	0.2	1.5	1.1	0.9
Ta	0.1	0.8	0.2	0.1	0.4	0.2				0.1	0.2	0.1	0.5	0.4	1.3
Nb	1.1	13.1	3.6	1.0	6.4	2.4				0.6	2.9	2.2	8.9	4.8	10.2
La	6.5	20.9	10.1	7.6	24.4	17.5	1.6	39.8	9.7	5.0	10.7	6.8	56.0	15.7	18.0
Ce	21.9	45.6	37.3	16.2	58.6	40.1				11.0	24.5	14.2	125.1	31.7	39.1
Pb		2.0					1.0	20.0	4.0		5.0		11.0	11.3	9.0
Pr	3.9	6.7	4.7	2.3	8.7	5.4				1.6	3.2	1.9	16.4	3.9	4.5
Sr	92.9	565.1	465.9	188.6	973.9	591.0	7.0	1160.0	475.0	140.9	874.0	514.3	844.4	173.2	240.0
Nd	18.6	34.0	22.7	9.7	40.1	23.2				5.8	14.1	7.2	65.9	14.5	16.8
Zr	30.1	184.3	44.6	29.5	89.3	34.9	0.5	313.0	39.0	10.1	70.4	33.2	165.1	125.2	143.0
Hf	1.1	5.2	1.7	1.1	2.6	1.1				0.4	1.9	0.9	4.5	3.1	3.8
Sm	3.5	8.9	6.0	2.2	9.0	5.2				1.1	3.1	1.7	12.6	2.8	4.0
Eu	1.1	2.5	1.5	0.9	2.8	1.7				0.5	1.1	0.9	3.0	0.8	0.9
Gd	3.3	7.6	5.3	2.4	7.5	4.9				1.2	2.8	1.8	9.3	2.6	3.9
Tb	0.5	1.1	0.7	0.4	0.9	0.7				0.2	0.4	0.3	1.1	0.4	0.7
Dy	2.7	6.0	3.5	2.6	4.2	3.8				0.8	2.2	1.6	4.9	2.7	4.3
Y	12.8	27.4	15.9	14.6	22.0	17.4	0.5	38.0	16.0	4.5	11.3	8.4	22.5	13.2	28.7
Ho	0.6	1.1	0.7	0.6	0.8	0.7				0.2	0.5	0.3	0.9	0.5	0.9
Er	1.5	2.9	1.6	1.6	2.4	1.7				0.4	1.3	0.9	2.1	1.6	2.6
Tm	0.2	0.4	0.3	0.2	0.4	0.2				0.1	0.2	0.1	0.3	0.2	0.4
Yb	1.1	2.2	1.4	1.4	2.4	1.5				0.4	1.1	1.0	1.8	1.5	2.9
Lu	0.2	0.3	0.2	0.2	0.3	0.2				0.1	0.2	0.1	0.3	0.2	0.4
V	268.1	966.0	424.1	213.5	341.0	289.8	16.0	2540.0	168.0	49.3	299.3	223.2	178.1	173.3	89.0
Sc	24.2	70.0	29.1	28.5	37.3	31.3	0.5	51.0	21.0	4.0	23.3	17.4	17.0	21.1	9.0
La/Sm	1.1	6.0	1.2	2.7	3.5	3.3				3.0	5.4	3.7	4.4	5.6	4.6
Gb/Yb	2.3	4.6	4.1	1.5	5.2	2.8				1.3	3.0	2.1	5.3	1.7	1.3
La/Yb	5.1	14.7	6.8	4.7	16.9	10.7				4.5	16.6	7.8	32.0	10.4	6.2
Ta/Yb	0.1	0.4	0.2	0.1	0.2	0.1				0.1	0.5	0.1	0.3	0.2	0.5
Th/Yb	0.1	2.9	0.4	0.1	0.9	0.2				0.1	1.3	0.4	3.7	2.9	2.3
Nb/Yb	1.0	5.9	2.8	0.7	2.7	1.6				0.5	7.1	2.3	5.1	3.2	3.5

Table 2 (continued)

	CPXYT ($n=5$)			MGAB ($n=4$)			GAB ($n=121$)*			LGAB ($n=5$)			LGAB-Bio ($n=1$)	MTSD ($n=1$)	Ton ($n=1$)
	Min	Max	Med	Min	Max	Med	Min	Max	Med	Min	Max	Med			
Ba/Th	78.2	439.5	189.7	115.7	3427.3	922.9				162.8	1775.0	922.2	131.4	95.8	49.6
Th/Nb	0.1	0.7	0.2	0.1	0.3	0.1				0.1	0.7	0.2	0.7	0.9	0.7
Th/La	0.0	0.2	0.1	0.0	0.2	0.0				0.0	0.2	0.0	0.1	0.3	0.4
Zr/Nb	10.3	27.3	14.1	13.1	29.0	15.6				13.3	24.1	18.3	18.5	26.2	14.1
Zr/Y	2.0	10.6	2.3	1.6	4.1	2.3			2.4	1.1	15.6	4.0	7.3	9.5	5.0
Zr/Hf	24.7	38.3	27.3	26.4	34.5	31.2				25.0	44.0	35.6	36.7	39.9	37.2
Eu/Eu*	0.6	1.1	0.8	1.0	1.3	1.1				1.1	1.6	1.4	0.9	0.9	1.1
Nb/Nb*	0.2	1.1	0.5	0.2	0.7	0.3				0.2	0.5	0.4	0.2	0.2	0.1
Sr/Sr*	0.2	1.6	1.2	0.8	1.6	1.5				1.2	6.3	3.0	0.7	0.6	0.9
Zr/Zr*	0.2	1.2	0.2	0.1	0.9	0.4				0.2	1.5	0.5	0.4	1.4	4.2
Ti/Ti*	0.6	1.3	1.0	0.4	1.0	0.7				0.8	1.5	1.0	0.4	0.8	0.9
Y/Ho*	0.8	0.9	0.8	0.9	0.9	0.9				0.8	1.0	0.9	0.9	0.9	0.9

Data shown here is compiled for the Impala Canada Ltd., geochemical database. All oxide concentrations are shown in wt%. All trace elements are shown in ppm

*Calculated using trace element data normalized with values of Sun and McDonough (1989)

†From Impala Canada Ltd., database

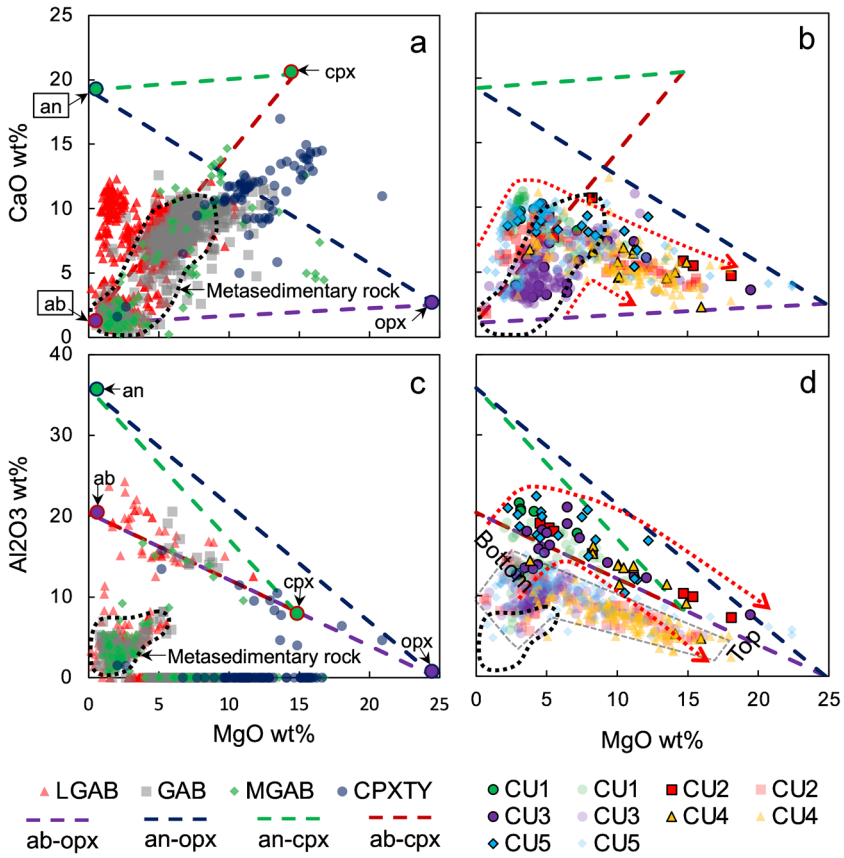

Fig. 5 Bivariate plots showing whole-rock major-element data from surface samples (**a** and **c**) and drill hole LL10-005 (**b** and **d**). Bimodal mixing lines for pure albite (ab)–orthopyroxene (opx), anorthite (an)–orthopyroxene (opx), anorthite–clinopyroxene (cpx), and albite–clinopyroxene are shown as dotted lines (see legend for details). The composition of Quetico metasedimentary rock is outlined with a black dotted line. Note that the misalignment between data from this study (symbols outlined in black in d and b) and data from the Impala Canada Ltd., geochemical database (semi-transparent symbols in d and b) in Al_2O_3 vs. MgO space (outlined with gray dotted line in "d") is the result of incomplete dissolution of aluminous mineral phases during the analysis obtained by Impala Canada Ltd

rocks that envelope the complex along its eastern edge. These data clusters within the primary group are observed in all major-element data (e.g., Na_2O, TiO_2, Fe_2O_3, Cr vs. MgO) from intrusive lithologies in the LLC.

The second group represents data from mineralized cyclic units and metasedimentary rock-bearing lithologies observed in drill hole LL10-005. These data points plot mostly between the orthopyroxene–albite and orthopyroxene–anorthite control lines, and can be visualized in Al_2O_3 and CaO vs. MgO space (Fig. 5b, d) as upward arcing arrays (between ~ 1.0 and 23.0 wt% Al_2O_3, ~ 2.0 and 12.0 wt% CaO, and ~ 1.0 and 16.0 wt% MgO), with an inflection point at ~ 5 wt% MgO. The low MgO segment of this array consists of samples from the bottoms of cyclic units (described below) and, in all cases, overlaps with the upper compositional range of the local Quetico metasedimentary rock. The higher MgO (~ 5.0–22.0 wt% MgO) segment of this array is representative of the middle and tops of the cyclic units identified in LL10-005, and occurs between the orthopyroxene–albite and orthopyroxene–anorthite control lines in CaO vs. MgO space and roughly parallel to, or slightly overlapping the orthopyroxene–albite control line in Al_2O_3 vs. MgO space.

Primitive-mantle normalized trace-element profiles of all lithologies (e.g. leucogabbro and clinopyroxenite; Fig. 6a, b) are nearly identical: they have strongly fractionated light REE (LREE; median primitive-mantle normalized La/Sm of 1.35–2.87) and heavy REE (HREE; median primitive-mantle normalized Gd/Yb of 1.67–4.37) patterns, are enriched in the fluid-mobile large-ion lithophile elements (LILE; Cs, Rb, Ba, and K) and Pb, have generally high Ba/Th ratios (median values of absolute concentrations: clinopyroxenite = 190, melanogabbro = 923, leucogabbro = 922), have Hf/Zr and Y/Ho ratios that are uniformly near unity, and have negative Nb (range of median Nb/Nb* of 0.16–0.45; $Nb/Nb^* = Nb_n/(Th_n \bullet La_n)^{0.5}$) and Zr anomalies (range of median Zr/Zr* of 0.22–0.45; $Zr/Zr^* = Zr_n/(Nd_n \bullet Sm_n)^{0.5}$). In addition, Th/Nb, Zr/Nb, and Zr/Y ratios are consistently near primitive mantle values (PM: 0.12, 15.96, and 2.44, respectively), varying within 1 order of magnitude or less (Table 2). However, Eu concentrations do show some variability between rock types and are positively correlated with estimated modal plagioclase abundances, with Eu/Eu* ($Eu/Eu^* = Eu_n/(Sm_n \bullet Gd_n)^{0.5}$) being slightly negative (median = 0.84) in clinopyroxenite, and moderately to strongly positive in melanogabbro (median = 1.07) and leucogabbro (median = 1.36). Likewise, Sr concentrations are variable across all rock types, but are typically strongly enriched in melanogabbro and leucogabbro (median Sr/Sr* = 1.94 and 2.97, respectively; $Sr/Sr^* = Sr_n/(Ce_n \bullet Nd_n)^{0.5}$), and mostly flat in clinopyroxenite (median Sr/Sr* = 1.17). Titanium is also highly variable, with Ti/Ti* ranging from positive to strongly negative (median Ti/Ti* of 0.37–1.10; $Ti/Ti^* = Ti_n/(Gd_n \bullet Dy_n)^{0.5}$).

The trace-element compositions of the sulfide-bearing cyclic units in the Northwestern Border Zone (Fig. 6c, d)

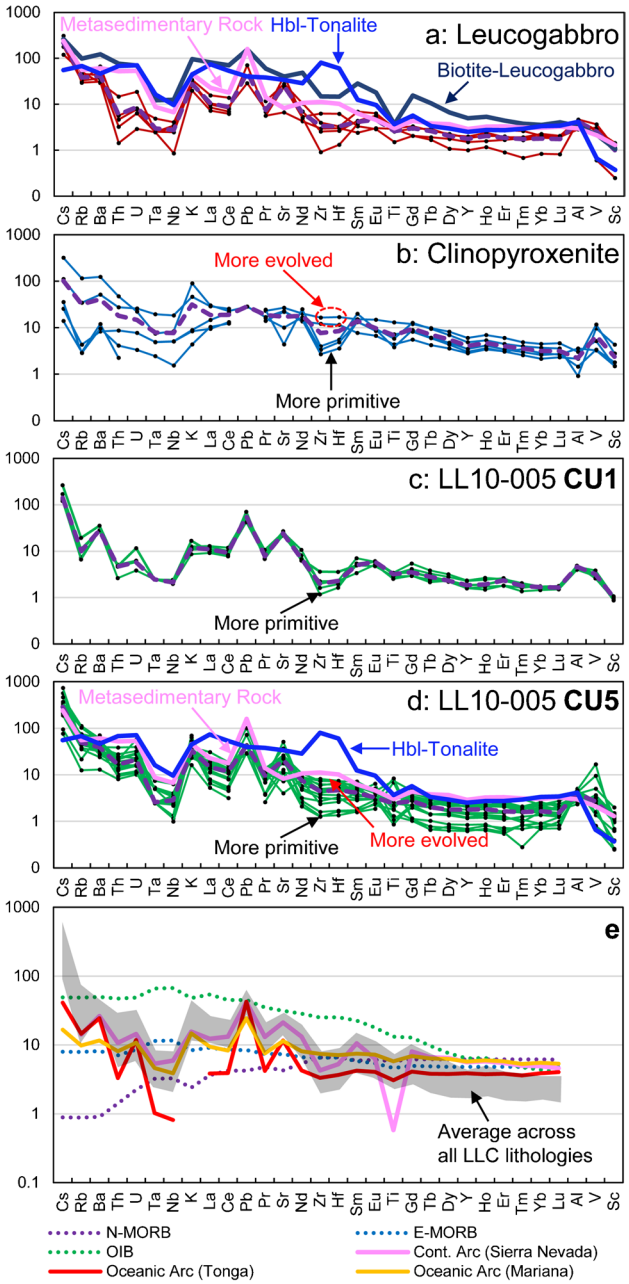

Fig. 6 Primitive mantle-normalized trace-element profiles for leucogabbro (**a**), clinopyroxene (**b**), and cyclic units from drill hole LL10-005 (**c**: CU1 and **d**: CU5). The average trace-element profile for LLC lithologies in each panel is shown as a purple dotted line in each panel. Profiles for Quetico metasedimentary rock (pink line) and Wabigoon hornblende-tonalite (yellow) are shown in "a" and "d." The trace-element profile for biotite-leucogabbro is shown in blue in "a." Note the contrast in the magnitude and polarity of Zr–Hf anomalies in Quetico metasedimentary rock, tonalite, and LLC lithologies. **e** Primitive mantle-normalized trace-element profiles for N-MORB, E-MORB, and OIB (Sun and McDonough 1989), continental arc gabbro (Sierra Nevada: McCarthy et al. 2016), and oceanic arc basalt (Tonga arc: Ewart and Hawkesworth 1987; Mariana arc: Yanhong et al. 2021) overlain on the average range of trace-element compositions of all lithologies in the LLC (gray field). Normalization values from Sun and McDonough (1989)

are similar to the unmineralized leucogabbbro elsewhere in the complex. These similarities include enrichment in the fluid-mobile lithophile elements (Cs, Rb, Ba, K; high absolute Ba/Th ratios, with median values of 144–615) and Pb, negative Nb and Zr anomalies (median Nb/Nb* = 0.15–0.33; median Zr/Zr* = 0.25–0.87), Hf/Zr and Y/Ho ratios that are uniformly near unity, flat to negative Ti/Ti* anomalies (median Ti/Ti* = 0.67–0.99), flat to strongly positive Eu/Eu* and Sr/Sr* anomalies (median Eu/Eu* and Sr/Sr* between 0.96–1.28 and 0.84–2.97), and Th/Nb, Zr/Nb, and Zr/Y ratios near that of the primitive mantle. However, the mineralized lithologies tend to have more fractionated LREE (median La/Sm_{pm} = 2.22–3.54) and HREE (median Gd/Yb_{pm} = 1.57–2.09) compositions.

A general feature of the trace-element data for all major lithologies is that the upper range of variability matches the composition and pattern of enrichment/depletion observed in the local Quetico metasedimentary country rock (e.g., Fig. 6a, d). This feature is particularly apparent in the cyclic units in which primitive mantle trace-element profiles occur along a continuum between more primitive profiles (closer to PM for most elements) with strongly negative Nb and Zr anomalies and more evolved profiles with more fractionated REE patterns and flatter Nb and Zr anomalies (Fig. 6d). Moreover, the paragenetically late biotite-leucogabbro has much more evolved composition with highly fractionated LREE (La/Sm_{pm} = 2.87) and HREE profiles (median Gd/Yb_{pm} = 4.34), but displays many of the same trends in trace-element depletion/enrichment as the Quetico metasedimentary country rock. These include similar Ba/Th ratios, Nb/Nb*, Sr/Sr*, and Ti/Ti*. However, the magnitude of the Zr/Zr* in the biotite-leucogabbro (0.40) is similar to the other lithologies in the LLC.

Sulfur, Se, PGE, and base-metal concentrations of surface samples from the LLC are summarized in Supplementary Table 5 in ESM2. Sulfide mineralization in the LLC is relatively sparse outside the Northwestern Border Zone, with concentrations of S, Se, Pd, Pt, Cu, and Au generally quite low across all lithologies (ESM2, Table 5), except in isolated zones of pyrite- and chalcopyrite-bearing leucogabbro and gabbro (up to 2.50 wt% S, 4.71 ppm Se, 1.40 ppm Pd, 0.53 ppm Pt, 5000 ppm Cu, and 1 ppm Au). In these zones, S–Cu and Pd–Pt are correlated with one another, consistent with the presence of chalcopyrite- and sulfide-associated PGE mineralization. More mafic lithologies (i.e., clinopyroxenite and melanogabbro) exhibit consistently lower metal concentrations relative to the more felsic lithologies (gabbro and leucogabbro), but have similar Pd/Pt ratios (range of median Pd/Pt across all lithologies: 1.17–1.71).

The highest concentrations of, and most clear correlation between, base and precious metals and S occur in the Northwestern Border Zone in the basal portions of cyclic units CU1 and CU5 (Fig. 4). Here the abundances of Cu, Pd, and S are strongly correlated with depth and the modal abundance of chalcopyrite (Fig. 7a, c). Palladium and Pt strongly correlate with one another in all lithologies (Fig. 7d) but form two groups of data points relative to the concentration of PGE-bearing mineralization: one with median Pd/Pt of 4.21–5.03 (CU1, CU2, CU5; Fig. 7d) and another with 0.85–1.71 (CU3, CU4; Fig. 7d). Palladium and Cu are positively correlated and mostly within the range of the primitive mantle (Fig. 7e) in CU1 and CU5. In contrast, Cu and Pd show little correlation in CU2–CU4 and, with the exception of CU2, data plot below the mantle range in Pd vs. Cu space (Fig. 7e). Cu/Pd ratios vary widely across all cyclic units (overall range: 235–128,800), with data from CU1 (median value of 4663) and CU5 (median value of 4381) falling within the range of the primitive mantle (~ 1000–10,000; Barnes et al. 1993), and CU2–CU4 forming a cluster at higher values (median values of 8029, 23,533, and 28,833, respectively; Fig. 7f). Similarly, S/Se ratios are above the mantle range (2632–4350; Eckstrand and Hulbert 1987) in CU2–CU4 (median values of 5735, 8220, and 8699, respectively), near the mantle range in CU5 (median value of 4542), and at or below the mantle range in CU1 (median value of 1902; Fig. 7f).

The concentration of Ni throughout the LLC is generally quite low (typically < 194 ppm in all rock types) and shows a strong positive correlation with MgO and little to no correlation with S (Fig. 7b). Departures from this trend are only observed in CU5 and CU1, where high Ni concentrations correlate with the presence of pentlandite in the sulfide assemblage. This is consistent with the correlation between S and Ni at S concentrations > 8000 ppm in CU1 and CU5 (Fig. 7b).

Sm–Nd isotope composition of sulfide-bearing cyclic units

Whole-rock Sm–Nd isotope data from cyclic units in drill hole LL10-005 and Quetico metasedimentary rock (this study) are summarized in Supplementary Table 6 in ESM2 and shown in Fig. 8. The εNd_T values for LLC lithologies and Quetico metasedimentary rock were calculated using a zircon U–Pb age of 2690.59 (± 0.77) Ma (this study) and ~ 2703 Ma (Davis et al. 1990), respectively. Cumulate lithologies from the LLC have εNd_T values between − 0.06 and + 1.34 with most samples having positive, mantle-like values (DePaolo 1988). The total range of εNd_T values for the LLC are within the overall range of the εNd_T values for the LDI system (recalculated from Brügmann et al. 1997; Fig. 8), but cluster at positive values similar to Wabigoon tonalite (+ 0.76 to + 1.43). Quetico metasedimentary rocks bracket the lower range of LLC data at − 0.28 and − 0.58. Samples from CU1 and CU5 (the most mineralized cyclic

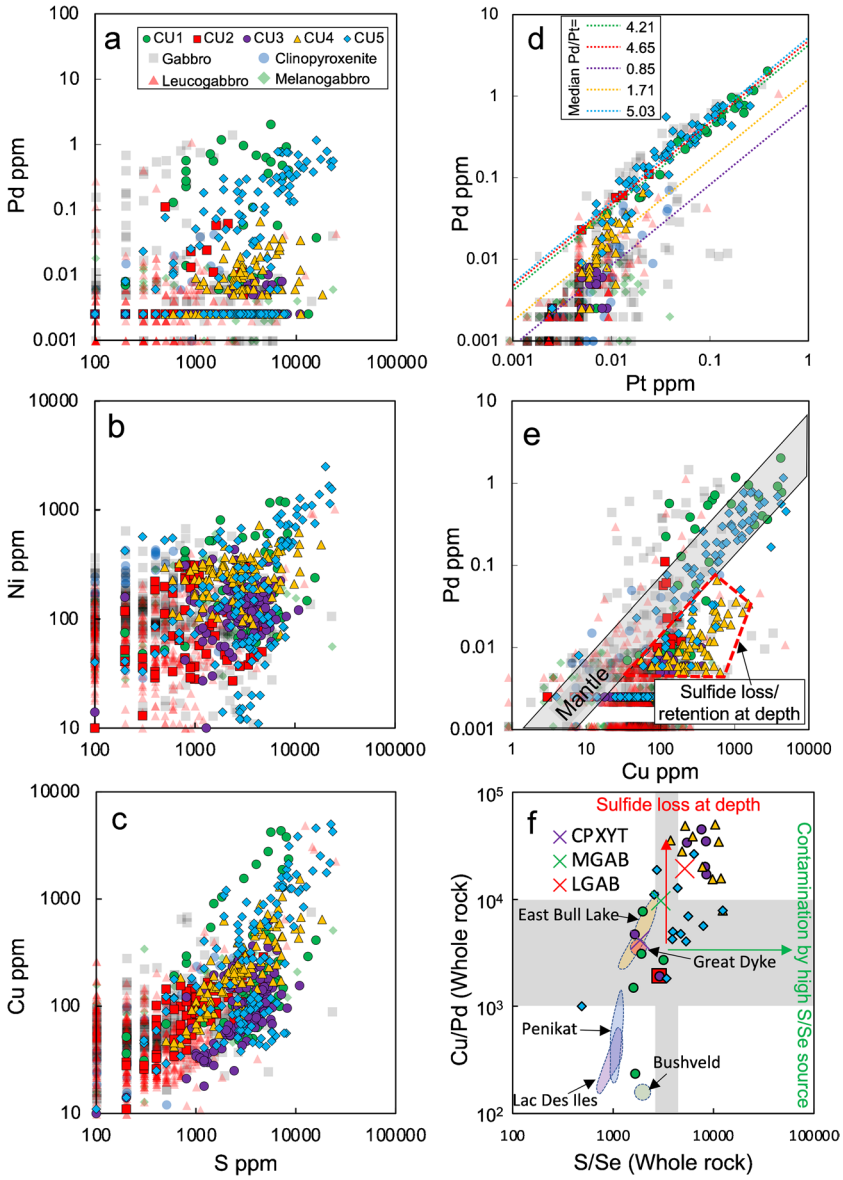

Fig. 7 Metal, S, and Se concentrations of whole-rock samples from mineralized cyclic units from drill hole LL10-005 (symbols outlined in black) and surface whole-rock samples from across the LLC (semi-transparent symbols). **a–c** Bivariate plots of whole-rock Pd, Ni, and Cu vs. S. Note that Ni concentrations are low in the LLC and are only correlated with S in CU1 and CU5 where pentlandite was observed. **d** Bivariate plots showing whole-rock Pd vs. Pt showing average Pd/Pt for each cyclic unit. **e** Bivariate plots showing whole-rock Pd vs. Cu. Mantle range from Barnes et al. (1993). **f** Comparison of whole-rock Cu/Pd and S/Se ratios. Gray field illustrates the mantle range of Cu/Pd and S/Se from Barnes et al. (1993; 1000–10,000) and Eckstrand and Hulbert (1987; 2632–4350), respectively. Colored fields represent the Cu/Pd vs. S/Se range of various other Ni–Cu–PGE deposits (after Brzozowski et al. 2020)

units) show the least variability relative to CU2–CU4 (Fig. 8) and are nearly identical range as that of the Wabigoon tonalite.

Sulfur isotopes

Multiple sulfur isotope data form pyrite, pyrrhotite, pentlandite, and chalcopyrite from the LLC are summarized in Table 3 (full data set in ESM2, Table 7). Figure 9 shows the average measured $\delta^{34}S$ values for individual sulfide grains by sulfide phase in each cyclic unit. The majority of the data points are within the mantle range ($0 \pm 1‰$; Sakai et al. 1984; Ripley and Li 2003; Seal 2006) and skew toward more positive values (Fig. 9a). No clear systematic difference is observed in the measured $\delta^{34}S$ that might indicate significant fractionation between sulfide phases. The average $\Delta^{33}S$ for individual sulfide grains across all sulfide phases are uniformly negative, non-zero values (Fig. 9b), and are beyond the range of variability that could arise for mass-dependent fractionation processes ($0 \pm 0.1‰$; Farquhar and Wing 2003). The average range of $\delta^{34}S$ values for Quetico metasedimentary rock are bracketed by the $\delta^{34}S$ values of mineralized intrusive rocks form the LLC (Fig. 10a). Likewise, the $\Delta^{33}S$ values for Quetico metasedimentary rock are also non-zero, but are less negative than most LLC cumulate lithologies.

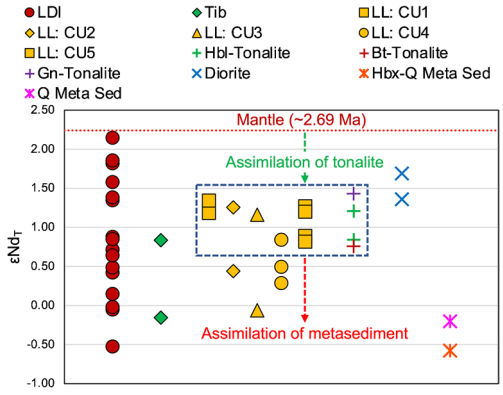

Fig. 8 Whole-rock εNd_T values for LDI, Tib Lake (Tib), and Wabigoon tonalite and Shelby Lake Diorite (from Brügmann et al. 1997) alongside that of the layered intrusive units from the LLC (yellow symbols) and Quetico metasedimentary rock (Q Meta Sed). Mantel value from Depaolo (1988). See legend for more details. εNd_T values for tonalite varieties (Gn = gneiss, Hbl = hornblende, Bt = biotite), Shelby Lake Diorite, and gabbroic rocks form the LDI systems were recalculated using Sm–Nd data from Brügmann et al. (1997) and average zircon U–Pb ages of ~ 2917–2728 Ma, ~ 2690 Ma, and ~ 2689 Ma, respectively (Ontario Geological Survey 2019)

Discussion

LDI and the LLC: Temporally associated intrusive complexes in a larger intrusive suite

The mafic–ultramafic systems of the LDI intrusive suite have similar petrographic and geochemical features, cross-cutting relationships with Archean host rocks, and NE-trending space cleavage parallel to the suture between the Wabigoon and Quetico Subprovinces (Stone 2010). These features suggest contemporaneous emplacement of the LDI intrusive suite during the subduction of the Wawa–Abitibi slab and formation of the Quetico Subprovince (Beakhouse and Davis 2005; Percival et al. 2012) following its accretion with the Wabigoon Subprovince at approximately 2.696–2.690 Ga (Williams 1990; Pettigrew and Hattori 2002; Stone 2010; Percival et al. 2012). When compared to the reported ages of the Mine Block Intrusion at LDI (2693.3 ± 1.3 Ma, and 2689.0 ± 1.0 Ma; Stone 2010) and the nearby Tib Lake Complex (2685.9 ± 1.6 Ma; Stone 2010), the U–Pb zircon age of 2690.59 ± 0.77 Ma for the LLC reported here is consistent with this interpretation, and indicates that the emplacement of the LDI intrusive suite was coeval with the formation of arc-related Alaskan-type ultramafic intrusions in the Quetico terrane (Pettigrew 2004). This suggests that the intrusive complexes of the LDI intrusive suite are also arc-related and part of a larger Archean arc-like setting.

Cyclic units in the LLC

The magmatic layering visible in downhole geochemical data from LL10-005 (Fig. 4) strongly resembles the cyclic units observed in many layered mafic intrusions globally (Great Dyke: Wilson and Prendergast 1989; Jimberlana intrusions: Campbell 1977; Duke Island Complex: Irvine 1974; Bushveld: Eales and Cawthorn 1996; Stillwater: McCallum 1996, Jackson 1961; Skaergaard: Boudreau and McBirney 1997; Sept Iles intrusion: Namur et al. 2010; North Lac De Iles: Djon et al. 2017a, b). A characteristic feature of cyclic units is the presence of systematic or repeating trends of element enrichment and depletion with depth that are truncated or reversed at the stratigraphic tops and bottoms of individual intrusive layers (Jackson 1961). This pattern reflects the formation of cyclic units by repeated injections of melt from a source reservoir and continuous fractionation at the site of emplacement with little external modification (Jackson 1961). A similar interpretation is applied to the cyclic units in the LLC (Fig. 4). However, a distinctive feature of the cyclic units in the LLC is that they are characterized by an upward modal increase in pyroxene rather than plagioclase. This is the opposite of what is commonly observed in cyclic units elsewhere (Campbell 1977) and likely relates to a systematic increase in SiO_2 activity via the progressive assimilation of Quetico metasedimentary rock fragments entrained in the intruding melt during emplacement (Campbell 1985). This is discussed in more detail in the following sections.

Mixing between compositionally distinct magmas prior to emplacement is a common process driving melt evolution in layered mafic systems (Maier 2005; Naldrett 2010, 2011; Mungall 2014), including LDI (Djon et al. 2017a, b). However, magma mixing does not appear to have occured during the formation of the LLC. This is illustrated by the consistent

Table 3 Summary of multiple sulfur isotope data from sulfides in drill hole LL10-005

LL10-005				Quetico metasedimentary rock		
LL10-005	δ34S‰	Δ33S (‰)	S/Se (WR)	LL10-005	δ34S‰	Δ33S (‰)
Min	−2.18	−0.41	2708.13	Min	−0.70	−0.17
Max	2.34	0.02	11,777.98	Max	1.16	0.02
Median	0.27	−0.15	4709.74	Median	0.07	−0.06

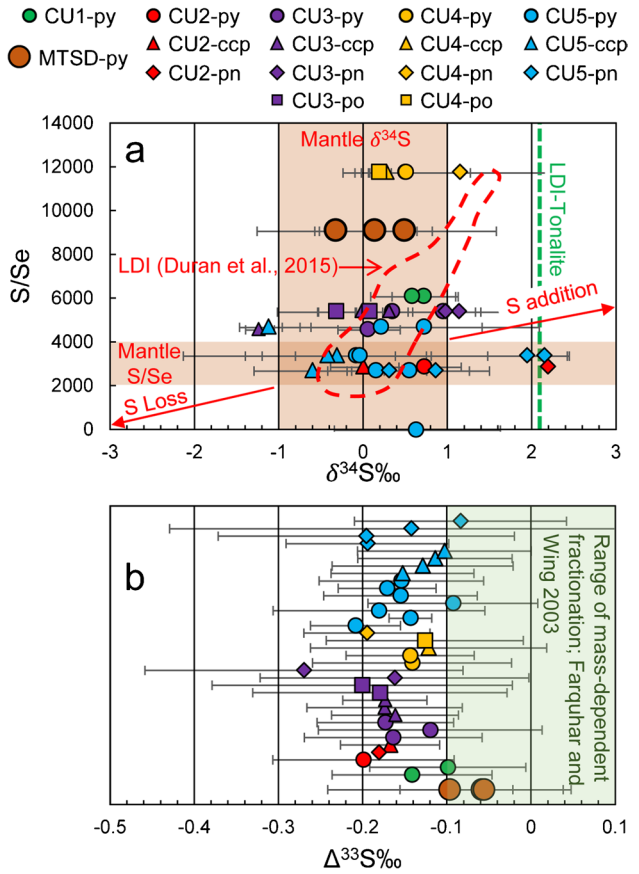

Fig. 9 **a** The $\delta^{34}S$ values for pentlandite (pn), pyrrhotite (po), chalcopyrite (ccp), and pyrite (py) from drill hole LL10-005 versus whole-rock S/Se data from the corresponding sulfide-bearing whole-rock samples (this study). Solid data points represent the average $\delta^{34}S$ value for individual sulfide grains. Mantle range of $\delta^{34}S$ and S/Se from Eckstrand and Hulbert (1987) and Farquhar and Wing (2003). The compositional range of sulfide pods and disseminated sulfides from LDI are outlined with a red dotted line (after Duran et al. 2015). $\delta^{34}S$ from LDI-tonalite from Jonsson (2023). Note that the S/Se (WR) of Quetico metasedimentary rock is 9109.47. **b** Range of $\Delta^{33}S$ ‰ for sulfides from drill hole LL10-005. Solid data points represent the average $\Delta^{33}S$ ‰ value for individual sulfide grains

sequence of crystallization relative to depth in individual cyclic units where the abundance of plagioclase increases with depth. This is consistent with the systematic decrease in MgO and CaO with depth (Fig. 4), and the low variability in incompatible trace-element compositions of LLC lithologies, which are sensitive tracers of magma source and evolution (Miller and Ripley 1996; Arndt et al. 2005; Maier 2005; Eckstrand and Hulbert 2007; Lightfoot 2007; Naldrett 2010, 2011; Mungall 2014; Charlier et al. 2015). For instance, magmas from contrasting source reservoirs are predicted to have contrasting Zr/Y ratios owing to the slightly differing incompatibilities of these elements (Pearce and Norry 1979). The range of Zr/Y ratios for LLC lithologies tightly overlap with less than an order of magnitude variability (Table 2; ESM2, Table 3). Together, this suggests that the formation of cyclic units in the LLC was indeed associated with nearly identical pulses of magma from a single parental source reservoir. Moreover, the parental melt appears to have had high SiO_2 and H_2O activity as suggested by the early crystallization of plagioclase and the presence of hydrous primary minerals such as biotite (Campbell 1985).

Mantle metasomatism prior to melt extraction

The strong enrichment of fluid-mobile incompatible trace elements (e.g., Cs, Rb, Ba; LILEs) in cumulate lithologies throughout the LLC could reflect a variety of processes, including hydrothermal alteration, crustal assimilation during emplacement, and mantle metasomatism. The possibility of LILE enrichment via hydrothermal alteration is supported by the presence of pervasive alteration in the Northwestern Border Zone, the general overprint of low temperature, chlorite-rich alteration throughout the LLC, and the observed variability in the relative abundances of LILEs and HFSE (e.g., K/Hf and Ba/Hf; ESM1, Fig. 3). However, this variability is highly localized to certain areas of the Northwestern Border Zone and is not representative of the LLC as a whole. For instance, the K/Hf and Ba/Hf ratios are strongly correlated in CU2–CU4 ($R^2 = 0.9$). In contrast, Ba is anomalously enriched in CU1 as is evident in its higher Ba/Hf ratios. LILE enrichment is ubiquitous throughout LLC lithologies, so the more common consistency of K/Hf and Ba/Hf ratios in most cyclic units suggests that LILE enrichment was a preexisting feature of LLC parental melts, and was variably overprinted by metasomatic LILE enrichment. Enrichment in LILE via crustal assimilation is supported by the clear textural and geochemical evidence of country rock assimilation in this system (e.g., Fig. 2a, b). However, variability in Ba/Th and Th/Nb ratios of the LLC lithologies, which can be modified by addition of LILE from metasomatic and crustal sources (Pirnia et al. 2020; Rahmani et al. 2020), indicates that this process likely overprinted existing LILE enrichment in LLC parental magmas prior to emplacement. In Ba/Th vs. Th/Nb space (ESM1, Fig. 4), crustal assimilation (i.e., Th addition) results in a range of Th/Nb ratios with little variation in Ba/Th, whereas addition of components by subduction-related fluids (e.g., Ba addition) produces the opposite pattern (Pirnia et al. 2020; Rahmani et al. 2020). Data points from the LLC show both patterns, with arrays parallel to the horizontal and vertical axes in Fig. 11 that converge near the origin. This pattern is hard to explain without the influence of both processes. In addition, Ba/La_{pm} and the magnitude of Sr anomalies are strongly correlated in lithologies throughout the LLC, whereas the magnitude of Eu anomalies and Al_2O_3 concentrations are less so (ESM1, Fig. 5). This pattern might reflect the presence of primary LILE-bearing hydrous minerals (i.e., amphibole and phlogopite) in the mantle source

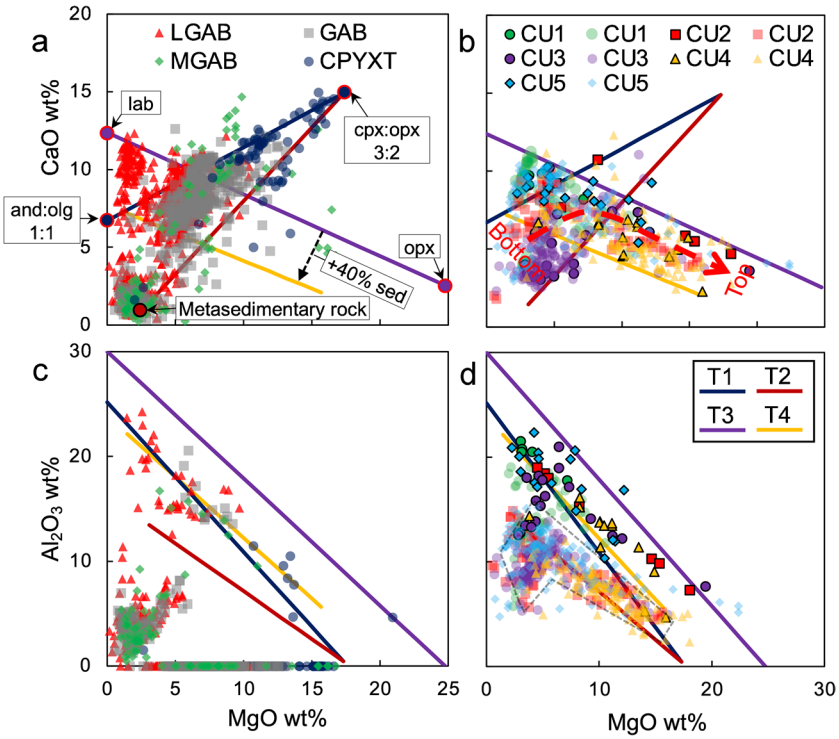

Fig. 10 Major element bivariate plots of whole-rock data (Impala Canada, Ltd.) from surface samples (**a** and **c**) and layered cyclic units in drill hole LL10-005 (**b** and **d**). Data from this study is shown as symbols outlined in black in b and d. Modeled mixing lines are shown as solid lines. See text for details

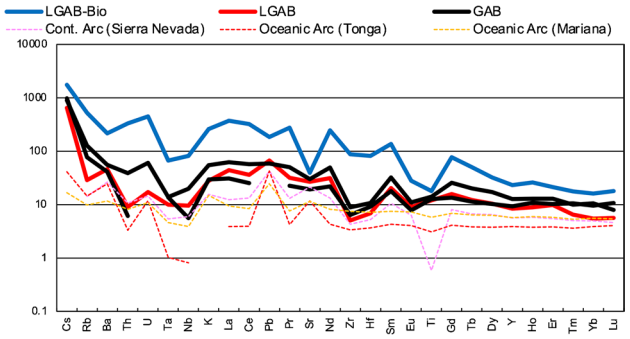

Fig. 11 Range of calculated parental melt compositions for major rock types in the LLC (solid lines). Example profiles of a modern continental arc gabbro (Sierra Nevada: McCarthy et al. 2016) and oceanic arc basalt (Tonga arc: Ewart and Hawkesworth 1987; Mariana arc: Yanhong et al. 2021) are shown as dotted lines. Note the similar pattern in enrichment but more evolved compositions of the calculated parental melts relative to the example profiles. Normalization values from Sun and McDonough (1989)

region formed via the addition of water prior to melt extraction (Good and Lightfoot 2019). This process is common in arc settings and is consistent with structural models of the southern Superior Province that suggest contemporaneous buckling of the Wawa–Abitibi slab and influx of mantle material during the formation of Alaskan-type ultramafic intrusions (which includes the LLC; Pettigrew 2004) in the Quetico Subprovince (Beakhouse and Davis 2005; Percival et al. 2012).

Crustal contamination

Mafic intrusions in the Superior Province commonly exhibit geochemical evidence of extensive crustal assimilation (Rudnick and Fountain 1995; Tomlinson et al. 1999; Hollings et al. 1999, 2007; Pearce 2008). In layered mafic systems, crustal assimilation is often a key driver of sulfide saturation and sulfide liquid immiscibility via the addition of external S or SiO_2 (Fiorentini et al. 2010; Naldrett 2011; Mungall 2014). A previous petrogenetic model for the LLC by Pettigrew and Hattori (2002) invoked the addition of external S and SiO_2 from assimilated metasedimentary rocks as the drivers of sulfide saturation and PGE mineralization. In contrast, sulfide melt immiscibility and extreme Pd enrichment in the LDI system is thought to be related to interactions between magmas and cumulate rocks with contrasting degrees of crustal contamination and S saturation at depth (Barnes and Gomwe 2011; Djon et al 2018). Thus, the nature of crustal contamination in the LLC and LDI systems likely influenced their relative PGE prospectivities.

The two most likely sources of crustal contamination in the LLC are Quetico metasedimentary rocks and Wabigoon tonalite. The LLC contains abundant evidence for extensive assimilation of Quetico metasedimentary rock. This is apparent in outcrop (Fig. 2a, b) and in the systematic variation of primitive mantle-normalized trace-element profiles from a more primitive, mantle-like profile to a more evolved profile that overlaps that of Quetico metasedimentary rock (Fig. 6c, d). In contrast, the hornblende-bearing tonalite

exhibits a distinctive trace-element profile relative to LLC lithologies characterized by a flat LILE pattern, a low Ba/Th_{pm} ratio, a strongly negative Nb/Nb* anomaly, fractionated LREE, and a strongly positive Zr/Zr* anomaly (relative to the LLC; Fig. 6a, d). Thus, the trace-element compositions of the cumulate lithologies suggest equilibration of the LLC magmas with Quetico metasedimentary rock rather than tonalite, with this process having played a key role in controlling the trace-element composition of the system. However, the systematic variability in trace-element data suggests that assimilation of, and equilibration with, Quetico metasedimentary rock was itself variable and likely occurred during emplacement at shallow levels. Had it occurred a depth where higher temperature conditions persisted and where melt was more actively mixed, the inheritance of its geochemical signature would have been more uniform across the LLC.

A key implication of the mixing patterns described above is that the more primitive profiles in Fig. 6a and d represent samples that partially preserve the initial geochemical and isotopic compositions of the primary melts in the LLC prior to emplacement. These samples have εNd_T values (Fig. 8; − 0.06 to + 1.34) that are close to that of Quetico metasedimentary rock (− 0.58 to − 0.20) at their negative extent, but cluster at a tight range of positive values (+ 0.82 to + 1.34) that are bracketed by that of the tonalitic country rock north and west of the LLC (Fig. 8; + 0.76 to + 1.43; Brügmann et al. 1997). This is particularly true in CU1, which does not exhibit textural or geochemical evidence of equilibration with Quetico metasedimentary rock (Fig. 5c), and has εNd_T values between + 1.18 and + 1.34. Based on this, we argue that the parental melts in the LLC initially had a mantle-like εNd_T (+ 2.44 at ~ 2.69 Ga; DePaolo 1988) and inherited the εNd_T signature of the tonalitic country rock at depth. During subsequent emplacement at shallow levels, variable assimilation of Quetico metasedimentary rock produced the more variable spread to negative εNd_T values in the LLC lithologies. This interpretation is supported by the fact that cyclic units with unambiguous geochemical and textural evidence for Quetico metasedimentary rock assimilation have the most variable and most negative εNd_T values (i.e., CU2–CU4), whereas those that lack this evidence consistently cluster at more positive values. It is possible that the spread in εNd_T values could arise solely from the mixing of mantle melts with Quetico metasedimentary rock; however, the observed clustering of data at positive values that are nearly identical to tonalitic country rock would be difficult to produce if this were the case. Moreover, the LLC occurs along the tectonic suture between the Quetico and Wabigoon Subprovinces, which would have served as a preferred pathway for the upward movement of silicate melts during the formation of the LLC and would have allowed for extensive interaction between all three components. Therefore, both crustal components likely contributed to the εNd_T signature of the LLC.

Sulfur saturation in the Legris Lake Complex

The concentration of sulfide mineralization at the bottoms of cyclic units and the high Cu/Pd ratios of unmineralized cyclic units (Fig. 6) are indicative of sulfide saturation prior to emplacement and loss of early formed sulfide liquid. This was driven by the addition of external sulfur as indicated by the high S/Se ratios (greater than that of the mantle range of Eckstrand and Hulbert 1987; 2632–4350), and corresponding positive $\delta^{34}S$ and non-zero $\Delta^{33}S$ values of the mineralized cyclic units (Fig. 9), which together provide robust constraints on the source of sulfur (Ripley and Li 2003; Penniston-Dorland et al. 2008; Sharman et al. 2013; Smith et al. 2016; Magalhães et al. 2019). The reliability of these constraints are due to the lower mobility of Se relative to S (Queffurus and Barnes 2015a, b), the distinctive isotopic signature of surface-derived material in the Archean (Farquhar and Wing 2003; Johnston 2011), and robustness of non-zero $\Delta^{33}S$ signatures during magmatic and metamorphic processes (Sharman et al. 2013). Most magmatic sulfides from the LLC have mantle-like $\delta^{34}S$ signature (Fig. 9a; $\delta^{34}S = 0 \pm 1‰$; Sakai et al. 1984; Ripley and Li 2003; Seal 2006), but skew towards more positive values. The corresponding S/Se ratios for each sample fall within or above the mantle range (Eckstrand and Hulbert 1987; Queffurus and Barnes 2015a, b). This is suggestive of crustal S addition (Smith et al. 2016) and is consistent with the uniformly non-zero $\Delta^{33}S$ values (between 0 and ~ − 0.3) of the sulfide mineralization. A non-zero $\Delta^{33}S$ signature is related to mass-independent fractionation of sulfur isotopes in the Archean atmosphere and are a well-defined tracer for Archean crustal inputs (Farquhar and Wing 2003; Seal 2006; Johnston 2011).

A comparison between the S/Se ratios and multiple sulfur isotope signature of LLC sulfide mineralization and the Quetico metasedimentary rock suggests that the latter is likely not the main source of external sulfur in the LLC. The average $\delta^{34}S$ signature of sedimentary pyrite in Quetico metasedimentary rock is within the range of the mantle and within the overall compositional range of magmatic sulfides in the mineralized cyclic units (Fig. 9a). A similar statement is true for the $\Delta^{33}S$ values of magmatic sulfides from the LLC, which are uniformly more negative than pyrite in Quetico metasedimentary rock (Fig. 9b). In both cases, the maximum range of error in the calculated sulfur isotope signature of the metasedimentary pyrite does not account for the range of variability in the average values or full range of error of the magmatic sulfides from the LLC. Moreover, the S/Se ratios of the metasedimentary pyrite are lower than the maximum S/Se ratio of the mineralized cyclic units (Fig. 9a). Together with the

observation that the abundance of sulfide mineralization is inversely correlated with Quetico metasedimentary rock assimilation in individual cyclic units, the metasedimentary material is likely not a key source of sulfur in this system. Rather, the tonalitic country rock is likely a more dominant source of external sulfur given its average $\delta^{34}S$ (+2.12; Jonsson 2023) that essentially overlaps the maximum $\delta^{34}S$ signature of the LLC (+2.15). This interpretation is also in good agreement with (i) the εNd_T signature of the LLC that is suggestive of tonalite assimilation at depth, (ii) the concentration of sulfide mineralization at the bottoms of cyclic units suggesting sulfur saturation prior to melt emplacement, and (iii) the S/Se and $\delta^{34}S$ signature of the LDI system that tightly overlaps the LLC data and in which tonalite is likely a dominant crustal contaminant (Duran et al. 2015; Fig. 10a).

Petrogenesis and mineralogy of the Legris system

Mixing with Quetico metasedimentary rock clearly influenced the major-element compositions of the intruding melts of the LLC. This effect must be accounted for when modeling the mineralogy of the LLC, and is illustrated in Fig. 10 using mixing lines between pure and contaminated mineral end-member assemblages. Melt emplaced at early stages in the LLC initially crystallized along a single trend (T1) that is modeled using an andesine and oligoclase end member (in 1:1 proportions) and a pyroxene end member (clinopyroxene and orthopyroxene in 3:2 proportions). This mixing line is representative of the least contaminated leucogabbro, gabbro, and clinopyroxenite. During each episode of melt injection at shallow levels, the fraction of assimilated Quetico metasedimentary rock was highly variable, producing compositional variation in the LLC lithologies that commonly overlaps with the composition of the Quetico metasedimentary rock. Samples of this type are represented by the data cluster near the origin in Fig. 10, and are modeled by a mixing line between pure Quetico metasedimentary rock and pyroxenite (clinopyroxene and orthopyroxene in 3:2 proportions; T2). The T1 and T2 mixing lines account for the end-member compositional variability observed in most of the unmineralized lithologies outside of the Northwestern Border Zone. Moreover, the area between T1 and T2 represents the variability in abundance and composition of plagioclase (between andesine and albite), and the relative abundance of metasedimentary material either as an assimilated component, xenolithic fragments, or a component of the heterolithic breccias.

Data points from the stratigraphic bottoms of cyclic units containing the mineralized leucogabbro and gabbro of the Northwestern Border Zone are closely bracketed by the low MgO ends of mixing lines T1 and T2. In contrast, data points from the stratigraphic middles and tops of mineralized cyclic units are closely bracketed in Fig. 10b and d by mixing lines representing combinations of pure labradorite and orthopyroxene (T3), and labradorite, orthopyroxene, and a constant 40 wt% contribution of Quetico metasedimentary rock (T4). The 40 wt% fraction of Quetico metasedimentary rock represents a maximum contribution of assimilated material in the mineralized cyclic units. It must be noted that data points between T3 and T4 in Fig. 10b and d are derived from samples in which Quetico metasedimentary rock assimilation is evident in hand sample and no discernible orthopyroxene is evident in thin section. A key point here is that the major-element chemistry of these samples is difficult to explain without a significantly larger input of assimilated metasedimentary material and a larger localized volume of orthopyroxene (up to ~ 19 wt%). A similar statement can be made about the LLC in general, with the caveat that the input of Quetico metasedimentary rock and the corresponding orthopyroxene abundance are lower outside of the Northwestern Border Zone. Moreover, the clear association between assimilated metasedimentary rock, and the occurrence of abundant orthopyroxene, and intergranular biotite and quartz in the middle parts and tops of the cyclic units suggests that assimilation of this material caused an increase in SiO_2 activity. This resulted in a localized shift toward a more orthopyroxene-dominated mineral assemblage as entrained metasedimentary material was progressively assimilated by fractionating silicate melt at the site of emplacement during the formation of the cyclic units (Campbell 1985). This localized effect accounts for the trend toward a more pyroxene-dominated (clinopyroxene–orthopyroxene) composition with decreasing depth in individual cyclic units in the LLC that is the opposite of the more typical trend toward higher modal plagioclase abundance with decreasing depth observed in cyclic units elsewhere.

The fact that orthopyroxene was not directly observed in any lithology other than the biotite-leucogabbro is likely due to the alteration of primary orthopyroxene to hornblende–actinolite–chlorite–epidote–talc. However, its occurrence implies that the LLC is dominantly gabbronoritic in composition rather than gabbroic as previously thought (Pettigrew and Hattori 2002). Similarly, olivine was not observed in any of the sampled lithologies. As with orthopyroxene, this does not preclude its occurrence. However, modeling of the whole-rock data provides clear evidence for an almost complete lack of olivine across all LLC lithologies, except for volumetrically minor zones of dunite encountered during drilling. This is consistent with the generally Ni-poor nature of all lithologies in the LLC and suggests that significant olivine crystallization occurred prior to emplacement.

Parental magma trace-element composition, tectonic setting, and magmatic evolution

The trace-element composition of cumulate rocks is not entirely representative of the composition of their parental melts (Barnes 1986; Godel et al. 2011). To account for this, we have applied the equilibrium distribution method (EDM; Bédard 1994, 2001, 2006) to model the composition of the parental melt of LLC cumulate rocks. Specific considerations used are described in detail in Tables 8 and 9 in ESM2. Whole-rock geochemical data used to model the parental melt compositions are from the least contaminated samples of leucogabbro, gabbro, and biotite-leucogabbro (LL10-005–47, LL10-005–117, LL-21–80, and LL-21-84a), with Hf/Zr and Y/Ho ratios near 1 (ESM1, Fig. 3), and minimal evidence of hydrothermal alteration. The contribution of trace elements from the trapped melt faction (TMF), which comprised the initial modal abundance of intergranular phases (2.8–13 vol.%; ESM2, Table 8) and variable proportions of mineral overgrowths on the primary cumulus phases, was subtracted using a non-modal melting approach ("backstripping"; Bédard 1994, 2001). A maximum final TMF of 20% was determined for mineralized leucogabbro based on the average abundance of intergranular minerals in samples from each lithology and the variability of model trace-element profiles produced with this value (Fig. 11). A maximum final TMF of 13% was determined for the biotite-leucogabbro and gabbro.

The calculated trace-element composition of parental melts for leucogabbro (CU1), gabbro (CU2 and surface sample), and biotite-leucogabbro (surface) are provided in Table 10 of ESM2 and illustrated in Fig. 11. The modeled parental melts for leucogabbro and gabbro closely overlap one another, and are characterized by fractionated LREE and HREE ($La/Sm_{pm} = 1.71–2.17$; $Gd/Yb_{pm} = 1.41–2.86$), uniform LILE enrichment, and negative Zr/Zr* (0.2–0.32), Eu/Eu* (0.39–0.51), Sr/Sr* (0.57–0.82), and Nb/Nb* (0.40–0.48) anomalies (Fig. 11). In contrast, the modeled parental magma for the biotite-leucogabbro is significantly more evolved, and features more negative Eu/Eu* (0.27), Sr/Sr* (0.14), Nb/Nb* (0.23), and Zr/Zr* (0.48) anomalies, and a greater degree of LREE ($La/Sm_{pm} = 2.72$) and HREE fractionation ($Gd/Yb_{pm} = 4.77$; Fig. 11). The modeled primitive mantle-normalized trace-element profiles of the mineralized leucogabbro and gabbro strongly resemble those of igneous rocks formed in modern arc settings, such as the Sierran continental arc (Fig. 11; Irvine and Baragar 1971; Pearce 1983; Barnes et al. 1993; Saccani et al. 2008). These similarities seem to support a model for the initial formation of the LLC involving discrete injections of a single parental magma formed via partial melting of metasomatized, LILE-enriched mantle in an arc setting in all but the very last stage of formation of the LLC. This interpretation is also in good agreement with data from the coeval LDI complex (Brügmann et al. 1997; Barnes and Gomwe 2011) and is suggestive of an arc setting for the LDI intrusive suite more broadly.

The more evolved composition of the calculated parental melt for the paragenetically late biotite-leucogabbro (Fig. 1b; Pettigrew and Hattori 2001) suggests that the parental melt reservoir feeding the system became more fractionated over time. This effect is likely due to the pervasive assimilation of Archean crustal material given the uniform enrichment in Th, and the resulting high Th/Yb, Th/Nb, and Th/La ratios of the calculated parental melts for biotite-leucogabbro (3.57, 0.49, and 0.11, respectively) relative to those for the calculated parental melts for mineralized leucogabbro (0.28, 0.11, and 0.03, respectively) and gabbro (0.11–0.63, 0.13–0.23, and 0.03–0.08, respectively). One effect of this assimilation would be the introduction of significant external SiO_2 to the melt prior to emplacement, and early crystallization and segregation of plagioclase and ferromagnesium minerals, such as orthopyroxene and olivine (Campbell 1985; Brügmann et al. 1997; Mungall 2014), which would have generated the negative Sr/Sr* and Eu/Eu* anomalies observed in all of the modeled parental melts, and the Ni-depleted character of the LLC. This process likely occurred throughout the evolution of the LLC and became more pervasive at later stages of evolution, leading to the more evolved composition of the biotite-leucogabbro. A key implication of this is that the parental magmas to the LLC resided at depth for some period of time prior to final emplacement, and crystallized a plagioclase-, orthopyroxene-, and olivine-bearing noritic cumulate pile either below the LLC or in the conduit system connecting the deep and shallow expressions of this system. This interpretation agrees with similar models for the LDI system in which noritic magmas were derived from a sub-plutonic reservoir (i.e., a staging chamber) where it interacted with additional compositionally distinct melts (Hinchey et al. 2005; Barnes and Gomwe 2011; Djon et al. 2017a, b).

Formation of the Legris Lake mafic–ultramafic complex

The data presented here indicate that the parental magmas to the LLC were likely initially extracted from a metasomatized mantle source in an arc setting. Following extraction, a single parental magma coalesced in a staging chamber where it assimilated external SiO_2 (Fig. 12) from tonalitic country rock, as suggested by the Sm–Nd isotope signature of the LLC. Introduction of external SiO_2 drove crystallization of olivine, orthopyroxene, and plagioclase prior to emplacement. This resulted in a bulk chemical change in the residual melt, producing a slightly more evolved composition with strongly negative Eu/Eu* and Sr/Sr* anomalies,

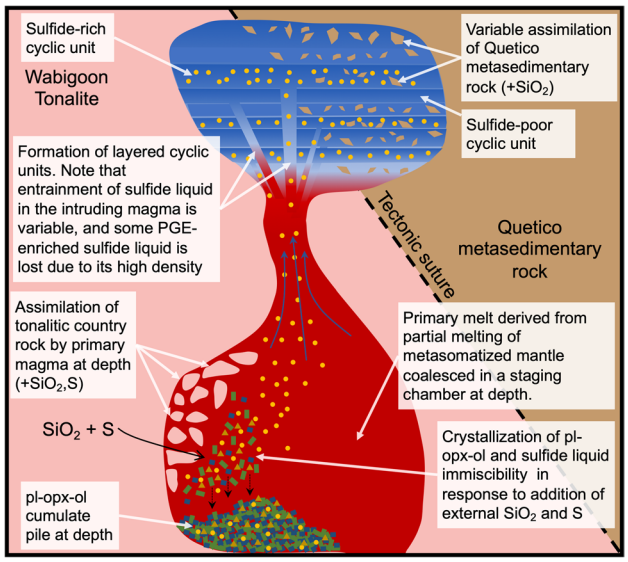

Fig. 12 Schematic diagram showing the formation of cyclic units in the Northwestern Border Zone (shown in blue) via injections of silicate melt that has assimilated SiO_2 and S from tonalitic country rock (pink) and evolved via crystallization of orthopyroxene (green rectangles), plagioclase (blue squares), and olivine (ol; brown triangles). Sulfide saturation occurred at depth or during emplacement and immiscible sulfide melt (yellow circles) was variably retained at the site of emplacement due to its high density. See text for details

highly fractionated REE profiles, and generally low Ni. This interpretation is similar to the genetic model for the LLC previously proposed by Pettigrew and Hattori (2001, 2002).

The sulfur isotope composition of the sulfide mineralization and whole-rock S/Se ratios suggest that addition of external S was a driver of sulfide liquid immiscibility in the LLC, likely due to the assimilation of tonalitic country rock. The segregation of sulfide liquid at the base of mineralized cyclic units (Fig. 4; CU1 and CU5) indicates that the intruding magmas were saturated with sulfide liquid at the time of emplacement. This early formed liquid would have efficiently stripped PGE from the coexisting silicate melt, but would have been difficult to mobilize in the intruding melts and retain at the site of emplacement due to its high density (4200–4500 kg/m^3; Dobson et al. 2000; Lesher 2019). As a result, the entrainment of PGE-rich sulfide liquid in individual magma pulses and its retention at the site of emplacement was variable, with some cyclic units having abundant PGE-bearing sulfide mineralization (CU1, CU5) and others having very little (CU2–CU4). Accordingly, the silicate melt that crystallized to form the latter group of cyclic units would have been relatively depleted in PGEs as a result of the loss of early formed sulfide liquid, resulting in elevated whole-rock Cu/Pd ratios (Fig. 7e, f).

Significant assimilation of Quetico metasedimentary rock at shallow levels drove a localized shift in melt composition, promoting orthopyroxene crystallization. This resulted in the more noritic composition of the stratigraphic middles and tops of cyclic units, and partial equilibration of the trace-element signatures of the silicate melt and metasedimentary rock. This also produced the observed compositional trend in cyclic units wherein they become more mafic and pyroxene-dominated with decreasing depth in response to the progressive assimilation of SiO_2 from abundant Quetico metasedimentary rock fragments entrained in intruding melts during the formation of individual cyclic units. However, this interaction was apparently unrelated to sulfur saturation.

The lack of trace-element variability between individual cyclic units suggests that the source and compositions of silicate melt pluses feeding the LLC remained relatively constant through most of its formation. However, over time assimilation of Quetico metasedimentary rock appears to have become more pervasive, resulting in a more Eu- and Sr- depleted, and LREE/HREE fractionated melt, with more evolved trace-element profiles similar to that of the metasediment. This is reflected in the mantle-normalized trace-element signature of the late-stage biotite-leucogabbro.

Comparison between the LDI Mine Block Intrusion and the LLC

In addition to the clear spatial and temporal association between the LLC and LDI, several other key similarities suggest a petrogenetic relationship between these systems, and perhaps a similar degree of PGE prospectivity.

1) The occurrence of large zones of brecciated and stratiform mineralization, with locally pervasive hydrothermal alteration (Barnes and Gomwe 2011).
2) Similar degrees of LILE enrichment and the occurrence of pegmatitic/varitextured rocks containing primary hydrous minerals (e.g., biotite, hornblende) indicative of melt extraction from a hydrous, metasomatized mantle source (Djon et al. 2018).
3) Similar trends of trace-element depletion and enrichment consistent with an arc setting (Brügmann et al. 1997; Barnes and Gomwe 2011; Djon et al. 2017a, b, 2018).
4) Similar ranges in S/Se ratios, and ^{34}S and εNd_T values in mineralized lithologies (Brügmann et al. 1997; Duran et al. 2015), and similar evidence of S and SiO_2 addition from Wabigoon tonalite.
5) Similar noritic composition and genetic models involving melt fractionation/crystallization at depth.

However, a key difference between LDI and the LLC is the role magma mixing played during the formation of each. In the LDI system, there is evidence for interactions between two compositionally distinct magmas involving the assimilation of early formed Pd-enriched sulfide mineralization by a secondary pulse of sulfide undersaturated melt. This likely drove sulfide

saturation in the secondary melt and resulted in a sulfide liquid with unusually high Pd/Pt ratios (Barnes and Gomwe 2011; Djon et al. 2017a, b, 2018). This sulfide liquid was subsequently emplacement and retained in the LDI Mine Block Intrusion. In contrast, magma mixing does not appear to have occurred during the magmatic evolution of the LLC and the early formed sulfide melt was only variably retained at the site of emplacement. This resulted in the more discrete volume of PGE-rich sulfide mineralization observed in the LLC relative to LDI.

Conclusion

Based on bulk-rock trace-element geochemistry and calculated parental melt compositions, the magmatic evolution of the LLC began with the partial melting of a metasomatized mantle source in an arc setting. Following the accumulation of this melt in a staging chamber, extensive assimilation of SiO_2 and S from tonalitic country rocks drove the crystallization of olivine, plagioclase, and orthopyroxene, and saturation of the melt in sulfide liquid. This, in turn, resulted in the formation of a more evolved, sulfide-saturated residual melt, with a tonalite-like εNd_T signature that was emplaced at shallow levels and crystallized the plagioclase-dominated cumulate lithologies of the LLC. Though not observed directly, orthopyroxene was a major part of the cumulate assemblage, indicating that the LLC is dominantly gabbronoritic rather than gabbroic in composition.

Mineralization in the LLC is primarily hosted in layered cyclic units that represent discrete pulses of a single parental melt. During their formation, entrainment of sulfide liquid during magma emplacement and its retention at shallow levels was variable due to the high density of the sulfide liquid. This led to variable degrees of PGE-rich sulfide mineralization among the cyclic units.

Variable assimilation of Quetico metasedimentary rock had a strong influence on the trace-element geochemistry of the LLC and resulted in a variable spread in the εNd_T signature of the cyclic units. This process drove a highly localized increase in the abundance of orthopyroxene, quartz, and biotite where metasedimentary rock was assimilated, and was most prevalent in the mineralized zones in the northwestern part of the LLC. However, the lack of correlation between metasedimentary rock assimilation and sulfide mineralization indicates that this was not an important factor in promoting sulfide saturation. Later in the evolution of the magmatic system, metasedimentary rock assimilation at depth became more widespread and exerted a stronger control on the trace-element geochemistry of this system.

The LLC and world-class LDI deposit share a clear temporal and geochemical association. Together with the Tib Lake Complex, they form a single intrusive suite that likely includes several other nearby PGE-bearing mafic–ultramafic complexes to the west and south (i.e., Wakinoo Lake, Demars Lake, Buck Lake, and Tamin Lake). Based on the model presented here, future studies should focus on the magmatic evolution of these systems and the processes driving sulfide saturation in each. Moreover, a detailed structural assessment to identify potential feeder conduits connecting the shallow and deeper level portions of these systems could provide key vectors to mineralization.

Supplementary Information The online version contains supplementary material available at https://doi.org/10.1007/s00126-023-01183-x.

Acknowledgements We thank Wolfgang Maier, Bernd Lehmann, Chris Jenkins, and an anonymous reviewer for their detailed critiques that greatly improved the final version of this manuscript. We also offer special thanks to Kristi Tavener and Jonas Valiunas for their help with sample preparation, Justin Jonsson and Tianna Groeneveld for the assistance in the field, and Devin Jackson and Jami Brown for the assistance in core sampling and mine site activities at LDI. We also thank Guosheng Wu, Shuangquan Zhang, Richard Stern, and Mike Hamilton for their assistance with analytical work and data collection.

Author contribution This manuscript and the data and interpretations presented herein were written by Dr. Wyatt M Bain. Dr. Peter Hollings oversaw this work and together with Dr. Matthew Brzozowski and Dr. Lionnel Djon provided assistance with field work and data presentation and interpretation and provided editorial support. Dr. Daniel Layton-Matthews and Dr. Agatha Dobosz carried out detailed MLA analysis of samples for this study and provided editorial support.

Funding This work was supported by Impala Canada Ltd., an NSERC Alliance grant (ALLRP 556281–20) and the NOHFC Industrial Research Chair to Hollings.

Declarations

Conflict of interest Author Lionnel Djon is currently an employee of Impala Canada Ltd. All other authors certify that they have no affiliations with or involvement in any organization or entity with any financial interest or non-financial interest in the subject matter or materials discussed in this manuscript.

References

Arndt N, Lesher CM, Czamanske GK (2005) Mantle-derived magmas and magmatic Ni-Cu-(PGE) deposits. Econ Geol 100th Anniversary volume, 5–23

Barnes SJ (1986) The effect of trapped liquid crystallization on cumulus mineral compositions in layered intrusions. Contrib Mineral Petrol 93:524–531

Barnes SJ, Picard CP (1993) The behavior of platinum-group elements during partial melting, crystal fractionation, and sulphide segregation: an example from the Cape Smith Fold Belt, northern Quebec. Geochim Cosmochim Acta 57:79–87

Barnes SJ, Gomwe TS (2011) The Pd-deposits of the Lac des Iles Complex, north-western Ontario. Rev Econ Geol 17:351–370

Barnes SJ, Couture JF, Sawyer EW, Bouchaib C (1993) Nickel copper occurrences in the Belleterre-Angliers belt of the Pontiac subprovince and the use of Cu-Pd ratios in interpreting platinum-group element distributions. Econ Geol 88:1402–1418

Barnes SJ, Cruden AR, Arndt N, Saumur BM (2016) The mineral system approach applied to magmatic Ni–Cu–PGE sulphide deposits. Ore Geol Rev 76:296–316

Beakhouse GP, Davis DW (2005) Evolution and tectonic significance of intermediate to felsic plutonism associated with the Hemlo greenstone belt, Superior Province, Canada. Precambrian Res 137:61–92

Bédard JH (1994) A procedure for calculating the equilibrium distribution of trace elements among minerals of cumulate rocks and the concentration of trace elements in the coexisting liquids. Chem Geol 118:143–153

Bédard JH (2001) Parental magmas of the Nain Plutonic Suite anorthosites and mafic cumulates: a trace element modelling approach. Contrib Mineral Petrol 141:747–771

Blackburn CE, John GW, Ayers JA, Davis DW (1991) Wabigoon Subprovince. In Geology of Ontario. Ontario Geological Survey. Special 4(Part 1):303–381

Boudreau AE, McBirney AR (1997) The Skaergaard Layered Series. Part III. Non-dynamic Layering. J Pet 38:1003–1020. https://doi.org/10.1093/petroj/38.8.1003

Brügmann GE, Reischmann T, Naldrett AJ, Sutcliffe RH (1997) Roots of an Archean Volcanic arc Complex: the Lac de Iles Area in Ontraio, Canada. Precambrian Res 81:223–239

Brzozowski MJ, Samson IM, Gagnon E, Good DJ, Linnen RL (2020) On the mechanisms for low-sulfide, high-platinum group element and high-sulfide, low-platinum group element mineralization in the Eastern Gabbro, Coldwell Complex, Canada: evidence from textural associations, S/Se values, and platinum group element concentrations of base metal sulfides. Econ Geol 115:355–384

Campbell IH (1977) A study of macrorhythmic layering and cumulate processes in the Jimberlana Intrusion, Western Australia, Part I: The upper layered series. J Petv 18:183–215

Campbell IH (1985) The difference between oceanic and continental tholeiites: a fluid dynamic explanation. Contrib Mineral Petrol 91:17–43

Charlier B, Namur O, Latypov R, Tegner C (2015) Layered intrusions. Springer, Dordrecht, Netherlands, p 748

Davis DW, Pezzutto F, Ojakangas RW (1990) The age and provenance of metasedimentary rocks in the Quetico Subprovince, Ontario, from single zircon analyses: implications for Archean. Earth Planetary Sci Lett 99:195–205 sedimentation and tectonics in the Superior Province

DePaolo DJ (1988) Neodymium isotope geochemistry. Springer, Berlin 1–187

Djon ML, Peck DC, Olivo GR, Miller JD, Joy B (2018) Contrasting styles of Pd-rich magmatic sulfide mineralization in the Lac des Iles Intrusive Complex, Ontario, Canada. Econ Geol 113:741–767

Djon LM, Miller JD, Olivo GR, Peck DC (2017a) Petrogenesis of cyclic units in the Northern Ultramafic Center of the Lac des iles Complex Ontario Canada. Can Min 55:349–374

Djon ML, Olivo GR, Miller JD, Peck DC, Joy B (2017b) Stratiform platinum-group element mineralization in the layered Northern Ultramafic Center of the Lac des Iles Intrusive Complex, Ontario, Canada. Ore Geol Rev 90:697–722

Dobson DP, Crichton WA, Vočadlo L, Jones AP, Wang Y, Uchida T, Rivers M, Sutton S, Brodholt J (2000) In situ measurement of viscosity of liquids in the Fe-FeS system at high pressures and temperatures. Am Mineral 85:1838–1842

Duran CJ, Barnes SJ, Corkery J (2015) Geology, petrography, geochemistry, and genesis of sulfide-rich pods in the Lac des Iles palladium deposits, western Ontario, Canada. Min Deps 51:509–532

Eales HV, Cawthorn RG (1996) The Bushveld Complex, In: Cawthorn RG (ed) Devs Pet, Volume 15. Elsevier, Amsterdam 181–229. https://doi.org/10.1016/S0167-2894(96)80008-X

Eckstrand OR, Hulbert LJ (1987) Selenium and the source of sulfur in magmatic nickel and platinum deposits (abs): geological Association of Canada–Mineralogical Association of Canada, Program with Abstracts, vol 12, p 40

Eckstrand OR, Hulbert LJ (2007) Magmatic nickel-copper-platinum group element deposits, in Goodfellow, W.D., ed., Mineral Deposits of Canada: A Synthesis of Major Deposit Types, District Metallogeny, the Evolution of Geological Provinces, and Exploration Methods: Geological Association of Canada, Mineral Deposits Division, Special Publication No. 5, p. 205-222

Ewart A, Hawkesworth CJ (1987) The Pleistocene-recent Tonga-Kermadec arc lavas: interpretation of ne isotopic and rare Earth data in terms of a depleted mantle source model. J Pet 28:495–530. https://doi.org/10.1093/petrology/28.3.495

Farquhar J, Wing BA (2003) Multiple sulfur isotopes and the evolution of the atmosphere. Earth Planet Sci Lett 213:1–13

Fiorentini ML, Beresford SW, Rosengren N, Barley ME, McCuaig TC (2010) Contrasting komatiite belts, associated Ni–Cu–(PGE) deposit styles and assimilation histories. Aust J Earth Sci 57:543–566

Godel B, Barnes SJ, Maier WD (2011) Parental magma composition inferred from trace element in cumulus and intercumulus silicate minerals: an example from the Lower and Lower Critical Zones of the Bushveld Complex, South-Africa. Lithos 125:537–552

Good DJ, Lightfoot PC (2019) Significance of the metasomatized lithospheric mantle in the formation of early basalts and Cu–platinum group element sulfide mineralization in the Coldwell Complex, Midcontinent Rift, Canada. Can J Earth Sci 56:693–714

Gupta VK, Sutcliffe RH (1990) Mafic-ultramafic intrusives and their gravity field: Lac des Iles area, northern Ontario. Geol Soc Am Bull 102:1471–1483

Hinchey JG, Hattori KH, Lavigne MJ (2005) Geology, petrology, and controls on PGE mineralization of the southern Roby and Twilight zones, Lac des Iles mine, Canada. Econ Geol 100:43–61

Hollings P, Wyman D, Kerrich R (1999) Komatiite–basalt–rhyolite volcanic associations in Northern Superior greenstone belts: significance of plume–arc interaction in the generation of the proto-continental Superior Province. Lithos 46:137–161

Hollings P, Hart T, Richarson A, MacDonald CA (2007) Geochemistry of the Mesoproterozoic intrusive rocks of the Nipigon Embayment, Northwestern Ontario: evaluating the earliest phase of rift development. Can J Earth Sci 44:1087–1110

Irvine TN, Baragar WR (1971) A guide to the chemical classification of the common igneous rocks. Can J Earth Sci 8:523–548

Irvine TN (1974) Petrology of the Duke Island ultramafic complex, southeastern Alaska. Geol Soc Am Mem 138:240

Jackson ED (1961) Primary textures and mineral associations in the ultramafic zone of the Stillwater complex, Montana. US Geol Surv Prof Pap 358:1–102

Johnston DT (2011) Multiple sulfur isotopes and the evolution of Earth's surface sulfur cycle. Earth Sci Rev 106:161–183

Jonsson J (2023) Petrogenesis of mineralized horizons in the Offset and Creek zones, Lac des Iles Complex, N. Ontario. Lakehead University, unpublished MSc thesis, 322p.

Lesher CM (2019) Up, down, or sideways: emplacement of magmatic Fe-Ni-Cu-PGE sulfide melts in large igneous provinces. Can J Earth Sci 56:756–773

Lightfoot PC (2007) Advances in Ni-Cu-PGE sulphide deposit models and implications for exploration technologies. Proceedings of Exploration 07: Fifth Decennial International Conference on Mineral Exploration pp 629–646

Magalhães N et al (2019) Multiple sulfur isotopes reveal a possible non-crustal source of sulfur for the Bushveld Province, southern Africa. Geology 47:982–986. https://doi.org/10.1130/G46282

Maier WD, Roelofse F, Barnes SJ (2003) The concentration of the platinum-group elements in South African komatiites: implications for mantle sources, melting regime and PGE fractionation during crystallization. J Pet 44:1787–1804

Maier WD (2005) Platinum-group element (PGE) deposits and occurrences: mineralization styles, genetic concepts, and exploration criteria. J Afr Earth Sci 41:165–191

McCallum IS (1996) The Stillwater Complex. In: Cawthorn RG (ed) Developments in Petrology, Volume 15, Elsevier, Amsterdam, pp 441–483, https://doi.org/10.1016/S0167-2894(96)80015-7

McCarthy A, Mintener O, Bouvier AS, Baumgartner LP (2016) Melt extraction zones in shallow arc plutons: insights from fisher lake Orbicules (Sierra Nevada, Western USA). J Pet 57:2011. https://doi.org/10.1093/petrology/egw068

Miller JD, Ripley EM (1996) Layered intrusions of the Duluth Complex, Minnesota, USA. In: Cawthorn RG (ed) Layered Intrusions. Elsevier, Amsterdam, pp 257–301

Mungall JE (2014) Geochemistry of magmatic ore deposits. In: Treatise on Geochemistry, 2nd edn, pp 195–218. https://doi.org/10.1016/B978-0-08-095975-7.01108-6

Naldrett AJ (2004) Magmatic sulfide deposits. Springer, Berlin Heidelberg

Naldrett AJ (2010) From the mantle to the bank: the life of a Ni-Cu-(PGE) sulfide deposit. S Afr J Geol 113:1–32. https://doi.org/10.2113/gssajg.113.1-1

Naldrett AJ (2011) Fundamentals of magmatic sulfide deposits. Revs Econ Geol 17:1–50

Namur O, Charlier B, Toplis MJ, Higgins MD, Liégeois JP, Vander Auwera J (2010) Crystallization sequence and magma chamber processes in the ferrobasaltic Sept Iles layered intrusion, Canada. J Petv 51:1203–1236

Ontario Geological Survey (2019) Geochronology Inventory of Ontario—2019; Ontario Geological Survey, Geochronology Inventory of Ontario—2019 (online database).

Paces JB, Miller JD (1993) Precise U-Pb ages of Duluth Complex and related mafic intrusions, northeastern Minnesota: geochronological insights to physical, petrogenetic, paleomagnetic and tectonomagmatic processes associated with the 1.1 Ga mid-continent rift system. J Geophys Res 98:13997–14013

Pearce JA, Norry MJ (1979) Petrogenetic implications of Ti, Zr, Y, and Nb variations in volcanic rocks. Contrib Mineral Petrol 69:33–47

Pearce JA (1983) Role of the sub-continental lithosphere in magma genesis at active continental margin. In: Hawkesworth CJ, Norry MJ (eds) Continental Basalts and Mantle Xenoliths. Shiva Publications, Cheshire, pp 230–249

Pearce JA (2008) Geochemical fingerprinting of oceanic basalts with applications to ophiolite classification and the search for Archean oceanic crust. Lithos 100:14–48. https://doi.org/10.1016/j.lithos.2007.06.016

Penniston-Dorland SC, Wing BA, Nex PAM, Kinnaird JA, Farquhar J, Brown M, Sharman E (2008) Multiple sulfur isotopes reveal a primary magmatic origin for the Platreef PGE deposit, Bushveld Complex, South Africa. Geology 36:979–982. https://doi.org/10.1130/G25098A.1

Percival JA, Williams HR (1989) The Quetico accretionary complex, Superior Province, Canada. Geology 17:23–25

Percival JA, Skulski T, Sanborn-Barrie M, Stott GM, Leclair AD, Corkery MT, Boily M (2012) Geology and tectonic evolution of the Superior Province, Canada. In: Percival JA, Cook FA, Clowe RM (eds) Tectonic Styles in Canada: The LITHOPROBE Perspective, vol 49. Geological Association of Canada, Special Paper, pp 321–378

Pettigrew NT (2004) Cu-Ni-PGE mineralization and petrogenesis of mafic-ultramafic intrusions in the western Quetico and Wabigoon subprovinces, northwestern Ontario, Canada. M.Sc. thesis, University of Ottawa, Ottawa, Ontario.

Pettigrew NT, Hattori KH (2001) Geology of the Palladium-rich Legris Lake Mafic-Ultramafic Complex, Western Wabigoon Subprovince, Northwestern Ontario. Can Inst Min Met Petrol 10:35–49

Pettigrew NT, Hattori KH (2002) Palladium–copper–rich PGE mineralization in the Legris Lake mafic ultramafic complex, western Superior Province of Canada. Trans Inst Min Met 111:B46–B57

Pirnia T, Saccani E, Torabi G, Chiari M, Gorican S, Barbero E (2020) Cretaceous tectonic evolution of the Neo-Tethys in Central Iran: evidence from petrology and age of the Nain-Ashin ophiolitic basalts. Geosci Front 11:57–81. https://doi.org/10.1016/j.gsf.2019.02.008

Queffurus M, Barnes SJ (2015a) A review of sulfur to selenium ratios in magmatic nickel-copper and platinum-group element deposits. Ore Geol Rev 69:301–324

Queffurus M, Barnes SJ (2015b) A review of sulfur to selenium ratios in magmatic nickel–copper and platinum-group element deposits. Ore Geol Revs 69:301–324

Rahmani F, Mackizadeh MA, Noghreyan M, Marchesi C, Garrido CJ (2020) Petrology and geochemistry of mafic and ultramafic cumulate rocks from the eastern part of the Sabzevar ophiolite (NE Iran): implications for their petrogenesis and tectonic setting. Geosci Front 11:2347–2364

Ripley E, Li C (2003) Sulfur isotope exchange and metal enrichment in the formation of magmatic Cu-Ni-(PGE) deposits. Econ Geol 98:635–641

Rudnick RL, Fountain DM (1995) Nature and composition of the continental crust—a lower crustal perspective. Revs Geophy 33:267–309

Saccani E, Photiades A, Beccaluva L (2008) Petrogenesis and tectonic significance of IAT magma-types in the Hellenide ophiolites as deduced from the Rhodiani ophiolites (Pelagonian zone, Greece). Lithos 104:71–84

Sakai H, Des Marais DJ, Ueda A, Moore JG (1984) Concentrations and isotope ratios of carbon, nitrogen, and sulfur in ocean-floor basalts. Geochim Cosmochim Acta 48:2433–2441. https://doi.org/10.1016/0016-7037(84)90295-3

Seal R (2006) Sulfur isotope geochemistry of sulfide minerals. Rev Mineral Geochem 61:633–677

Sharman ER, Penniston-Dorland SC, Kinnaird JA, Nex PAM, Brown M, Wing BA (2013) Primary origin of marginal Ni-Cu-(PGE) mineralization in layered intrusions: Δ33S evidence from the Platreef, Bushveld, South Africa. Econ Geol 108:365–377. https://doi.org/10.2113/econgeo.108.2.365

Smith JW, Holwell DA, McDonald I, Boyce AJ (2016) The application of S isotopes and S/Se ratios in determining ore-forming processes of magmatic Ni–Cu–PGE sulfide deposits: a cautionary case study from the northern Bushveld Complex. Ore Geol Rev 73:148–174

Stone D (2010) Precambrian geology of the central Wabigoon Subprovince area, northwestern Ontario. Ontario Geological Survey, Open File Report 5422:1–130

Stone D, Lavigne MJ, Schnieders B, Scott J, Wagner D (2003) Regionalgeology of the Lac des Iles area. Ontario Geological Survey, Open File Report 6120, pp1-25

Sun SS, McDonough WF (1989) Chemical and isotopic systematics of oceanic basalts: implications for mantle composition and processes. Geol Soc Lond Spec Publ 42:313–345

Sutcliffe RH, Sweeny JM, Edgar AD (1989) The Lac des Iles Complex, Ontario: petrology and platinum-group elements mineralization in an Archaean mafic intrusion. Can J Earth Sci 26:1408–1427

Sutcliffe RH (1986) Regional geology of the Lac des Iles area, District of Thunder Bay. Ontario Geological Survey, Miscellaneous Paper 132:70–75

Tomlinson KY, Hughes DJ, Thurston PC, Hall RP (1999) Plume magmatism and crustal growth at 2.9 to 3.0 Ga in the Steep Rock and Lumby Lake area, Western Superior Province. Lithos 46:103–136

Williams HR (1990) Subprovince accretion tectonics in the southcentral Superior Province. Can J Earth Sci 27:570–581

Wilson AH, Prendergast MD (1989) The Great Dyke of Zimbabwe: I: Tectonic setting, stratigraphy, petrology, structure, emplacement and crystallization. In: Prendergast MD, Jones MJ (eds) Magmatic Sulphides — The Zimbabwe Volume. Institute of Mining & Metallurgy, London, pp 1–20

Yanhong C, Yaoling N, Qiqi X, Yajie G, Castillo PR (2021) An iron isotope perspective on back-arc basin development: messages from Mariana trough basalts. Earth Planet Sci Lett 572 https://doi.org/10.1016/j.epsl.2021.117133